arXiv:hep-ph/9601211v1 4 Jan 1996

DESY 95-249
December 1995

Real next-to-leading corrections to the multigluon amplitudes in the helicity formalism

Vittorio Del Duca
Deutsches Elektronen-Synchrotron
DESY, D-22603 Hamburg , GERMANY[1]

Abstract

Using the helicity formalism, we compute the corrections to the tree-level multigluon amplitudes in the high-energy limit, induced by the corrections to the multi-Regge kinematics, and we show that they coincide with the corresponding Fadin-Lipatov amplitudes at fixed helicities.

---

[1] After January 1, 1996: Dept. of Physics and Astronomy, University of Edinburgh, Edinburgh EH9 3JZ, Scotland

1 Introduction

The Fadin-Kuraev-Lipatov (FKL) multigluon amplitudes [1], [2] are the building blocks of the Balitsky-Fadin-Kuraev-Lipatov (BFKL) theory [3], which describes the dynamics of a short-distance strong-interaction process in the limit of high squared parton center-of-mass energy $\hat{s}$ and fixed momentum transfer $\hat{t}$. In the BFKL theory, the leading logarithmic contributions, in $\ln(\hat{s}/\hat{t})$, to the scattering amplitude with exchange of a color-singlet two-gluon ladder in the crossed channel are computed. At $\hat{t} = 0$ the amplitude is related via the $\hat{s}$-channel unitarity to the total parton cross section with exchange of a one-gluon ladder.

The FKL multigluon amplitudes are computed in the multi-Regge kinematics, which requires that the final-state gluons are strongly ordered in rapidity and have comparable transverse momentum. They assume a simpler analytic form when the helicities of the incoming and the outgoing gluons are explicitly fixed [4] and [5]. In addition, in ref. [5] it was shown that at the tree level, and for the helicity configurations they have in common, the FKL amplitudes coincide with the Parke-Taylor (PT) amplitudes [6] computed in the multi-Regge kinematics.

The BFKL theory has several phenomenological applications, among which to the evolution of the F_2 structure function in deeply inelastic scattering in the small x_{bj} regime [7], and to the behavior of the dijet production cross section at large rapidity intervals in hadron-hadron collisions [8]. The phenomenology, however, is limited from large theoretical uncertainties, due to the lack of knowledge of the next-to-leading logarithmic corrections to the BFKL theory. Accordingly, real next-to-leading corrections

[9], [10], [11] induced by the corrections to the multi-Regge kinematics, and virtual next-to-leading-logarithmic corrections [10], [12] to the FKL amplitudes have been computed. The real next-to-leading corrections, once integrated over the phase space, will yield the real next-to-leading-logarithmic corrections to the BFKL equation.

The corrections to the tree-level FKL amplitudes [9], [10], [11] arise from the kinematical regions in which two gluons or a quark-antiquark pair are produced with likewise rapidity, either at the ends of or along the ladder, which we term the forward-rapidity and the central-rapidity regions, respectively. The goal of this paper is to reexamine the purely gluonic corrections [9] to the tree-level FKL amplitudes from the standpoint of the helicity formalism.

In sect. 2 we summarize the contents of ref. [5], namely the computation of the FKL amplitudes in the helicity formalism and their equivalence to the PT amplitudes in the multi-Regge kinematics. In sect. 3 we compute the next-to-leading corrections to the FKL amplitudes in the forward-rapidity region: *a*) by using the helicity formalism, i.e. by specifying the PT amplitudes to the kinematics with two gluons produced with likewise rapidity in a forward-rapidity region (sect. 3.1); *b*) by fixing the helicities in the Fadin-Lipatov amplitudes [9] (sect. 3.2). The amplitudes, computed in the two different ways, coincide and have a fairly simple analytic form at fixed helicities. As a bookkeeping device to list the leading color configurations we have found useful the two-sided lego-plot picture [13] which we used extensively in the multi-Regge kinematics [5] and [14]. In sect. 4 we consider the next-to-leading corrections to the FKL amplitudes in the central-rapidity region. In the helicity formalism, the PT amplitudes allow us to compute the configurations with the two gluons in the central-rapidity region produced with equal helicity (sect. 4.1), however to analyse the case in which the two central gluons have opposite helicities we must consider the amplitudes with 3 negative-helicity gluons [15], [16] (sect. 4.2). In sect. 4.3 we fix the helicities in the Fadin-Lipatov amplitudes and show that they coincide with the respective amplitudes in the helicity formalism (sect. 4.1 and 4.2). We note, though, that both for the corrections in the forward-rapidity (sect. 3) and in the central-rapidity (sect. 4) regions, the algebra involved is simpler starting from the helicity amplitudes than by fixing the helicities in the Fadin-Lipatov amplitudes. In sect. 5 we summarize the results of this paper and present our conclusions.

2 The multigluon amplitudes in the multi-Regge kinematics in the helicity formalism

We consider the production of $n+2$ gluons of momentum p_i, with $i = 0, ..., n+1$ and $n \geq 0$, in the scattering between two gluons of momenta p_A and p_B, and we assume that the produced gluons fulfill the multi-Regge kinematics, i.e. we require that the gluons are strongly ordered in rapidity y and have comparable transverse momentum,

$$y_0 \gg y_1 \gg ... \gg y_{n+1}; \qquad |p_{i\perp}| \simeq |p_\perp| \,. \tag{1}$$

The tree-level amplitude for the production of $n+2$ gluons in the multiregge kinematics has been computed in ref.[2] (Fig.1),

$$\begin{aligned} iM^{ad_0\ldots d_{n+1}b}_{\nu_A\nu_0\ldots\nu_{n+1}\nu_B} &= 2i\,\hat{s}\left(ig\,f^{ad_0c_1}\,\Gamma^{\mu_A\,\mu_0}\right)\,\epsilon^{\nu_A *}_{\mu_A}(p_A)\epsilon^{\nu_0}_{\mu_0}(p_0)\,\frac{1}{\hat{t}_1} \\ &\times \left(ig\,f^{c_1d_1c_2}\,C^{\mu_1}(q_1,q_2)\right)\,\epsilon^{\nu_1}_{\mu_1}(p_1)\,\frac{1}{\hat{t}_2} \\ &\times \end{aligned} \tag{2}$$

$$
\begin{aligned}
&\times \\
&\times \quad \Big(ig\, f^{c_n d_n c_{n+1}}\, C^{\mu_n}(q_n, q_{n+1})\Big)\ \epsilon^{\nu_n}_{\mu_n}(p_n)\, \frac{1}{\hat{t}_{n+1}} \\
&\times \quad \Big(ig\, f^{b d_{n+1} c_{n+1}}\, \Gamma^{\mu_b\, \mu_{n+1}}\Big)\ \epsilon^{\nu_B *}_{\mu_B}(p_B)\epsilon^{\nu_{n+1}}_{\mu_{n+1}}(p_{n+1})\,,
\end{aligned}
$$

where $a, d_0, ..., d_{n+1}, b$, and $\epsilon_A, \epsilon_0, ..., \epsilon_B$ are respectively the colors and the polarizations of the gluons, the ν's are the helicities, the q's are the momenta of the gluons exchanged in the $\hat{t}$ channel, and $\hat{t}_i = q_i^2 \simeq -|q_{i\perp}|^2$. The Γ-tensors [2] are,

$$
\begin{aligned}
\Gamma^{\mu_A\mu_0}(p_A, p_0, p_B) &= g^{\mu_A\mu_0} - \frac{p_A^{\mu_0} p_B^{\mu_A}}{p_A\cdot p_B} - \frac{p_B^{\mu_0} p_0^{\mu_A}}{p_0\cdot p_B} + p_B^{\mu_0} p_B^{\mu_A}\, \frac{p_A\cdot p_0}{p_A\cdot p_B\, p_0\cdot p_B}\,, \qquad (3) \\
\Gamma^{\mu_B\mu_{n+1}}(p_B, p_{n+1}, p_A) &= g^{\mu_B\mu_{n+1}} - \frac{p_A^{\mu_B} p_B^{\mu_{n+1}}}{p_A\cdot p_B} - \frac{p_A^{\mu_{n+1}} p_{n+1}^{\mu_B}}{p_A\cdot p_{n+1}} + p_A^{\mu_{n+1}} p_A^{\mu_B}\, \frac{p_B\cdot p_{n+1}}{p_A\cdot p_B\, p_A\cdot p_{n+1}}\,,
\end{aligned}
$$

and the Lipatov vertex [1] is

$$
C^\mu(q_i, q_{i+1}) = \left[(q_i + q_{i+1})^\mu_\perp - \left(\frac{\hat{s}_{Ai}}{\hat{s}} + 2\frac{\hat{t}_{i+1}}{\hat{s}_{Bi}}\right) p_B^\mu + \left(\frac{\hat{s}_{Bi}}{\hat{s}} + 2\frac{\hat{t}_i}{\hat{s}_{Ai}}\right) p_A^\mu\right]\,, \qquad (4)
$$

with $q^\mu_{i\perp} = (0, 0; q_{i\perp})$ and the Mandelstam invariants as given by eq.(104) (Appendix B). The Γ-tensors and the Lipatov vertex are gauge invariant,

$$
\begin{aligned}
\Gamma^{\mu_A\mu_0}(p_A, p_0, p_B)\, p_0^{\mu_0} &= \Gamma^{\mu_A\mu_0}(p_A, p_0, p_B)\, p_A^{\mu_A} = 0 \qquad (5) \\
C(q_i, q_{i+1})\cdot p_i &= 0\,,
\end{aligned}
$$

making thus the amplitude (2) invariant with respect to arbitrary gauge transformations. The Γ-tensors conserve the helicity at the production vertices for the first and the last gluon along the ladder. The square of the Lipatov vertex (4), which forms the kernel of the BFKL equation [3], is

$$
\begin{aligned}
&C^\mu(q_i, q_{i+1}) C^{\mu'}(q_i, q_{i+1}) \sum_\nu \epsilon^\nu_\mu(p_i)\epsilon^{\nu *}_{\mu'}(p_i) \qquad (6) \\
&= -C^\mu(q_i, q_{i+1}) C^{\mu'}(q_i, q_{i+1}) g_{\mu\mu'} = 4\, \frac{|q_{i\perp}|^2 |q_{i+1\perp}|^2}{|p_{i\perp}|^2}\,,
\end{aligned}
$$

using the gauge invariance. Thus in the square (6) of the Lipatov vertex several cancellations have occurred, making the square of the vertex simpler than the vertex itself. One of the goals in using the helicity formalism, which we now turn to, is to achieve the simplicity of eq.(6) already at the amplitude level.

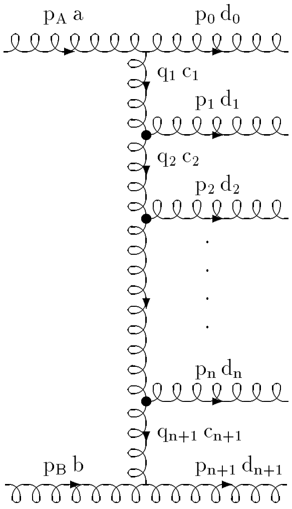

Figure 1: Multigluon amplitude in multiregge kinematics at the tree level. The blobs remind that non-local effective Lipatov vertices are used for the gluon emissions along the ladder.

2.1 The Fadin-Kuraev-Lipatov amplitudes at fixed helicities

We choose the representation (93) (Appendix A) for the polarizations. This is equivalent to use a physical gauge. Accordingly, we must specify a reference vector with respect to which we compute the polarizations in eq.(2), but thanks to the gauge invariance the choice is arbitrary. The contraction of the Lipatov vertex with the gluon polarization in eq.(2) is [4], [5],

$$\epsilon^{+}(p_i,p_A)\cdot C(q_i,q_{i+1}) = \sqrt{2}\,\frac{q^*_{i\perp}q_{i+1\perp}}{p_{i\perp}}\,. \tag{7}$$

From eq.(95) (Appendix A), the contractions of the helicity-conserving tensors (3) with the gluon polarizations are,

$$\begin{aligned} \Gamma^{\mu_B\mu_{n+1}}\,\epsilon^{+*}_{\mu_B}(p_B,p_A)\,\epsilon^{+}_{\mu_{n+1}}(p_{n+1},p_A) &= -\frac{p^*_{n+1\perp}}{p_{n+1\perp}}\,, \\ \Gamma^{\mu_A\mu_0}\,\epsilon^{+*}_{\mu_A}(p_A,p_B)\,\epsilon^{+}_{\mu_0}(p_0,p_B) &= -1\,. \end{aligned} \tag{8}$$

The product of the structure constants in eq.(2) may be rewritten as a trace of nested commutators of λ matrices, the color matrices in the fundamental representation of SU(N_c)

$$\begin{aligned} & f^{ad_0c_1}\,f^{c_1d_1c_2}\,\cdots f^{c_nd_nc_{n+1}}f^{bd_{n+1}c_{n+1}} \\ &= -2\,(-i)^{n+2}\,\mathrm{tr}\left(\lambda^a\,\left[\lambda^{d_0},\left[\lambda^{d_1},...,\left[\lambda^{d_{n+1}},\lambda^b\right]\right]\right]\right) \\ &= -2\,(-i)^{n+2}\,\mathrm{tr}\Bigg(\lambda^a\lambda^{d_0}\cdots\lambda^{d_{n+1}}\lambda^b - \sum_{j=0}^{n+1}\lambda^a\lambda^{d_0}\cdots\lambda^{d_{j-1}}\lambda^{d_{j+1}}\cdots\lambda^{d_{n+1}}\lambda^b\lambda^{d_j} \\ &+ \sum_{j<k}\lambda^a\lambda^{d_0}\cdots\lambda^{d_{j-1}}\lambda^{d_{j+1}}\cdots\lambda^{d_{k-1}}\lambda^{d_{k+1}}\cdots\lambda^{d_{n+1}}\lambda^b\lambda^{d_k}\lambda^{d_j}+\cdots\Bigg)\,. \end{aligned} \tag{9}$$

Substituting eq.(7), (8) and (9) into eq.(2), the FKL amplitude for the configuration with all the gluons having helicity $\nu=+$ becomes,

$$\begin{aligned} & iM(p_A,+;p_0,+;...;p_{n+1},+;p_B,+) \\ &= i(-1)^{n+1}\,2^{2+n/2}\,g^{n+2}\,\hat{s}\,\frac{1}{\prod_{i=0}^{n+1}p_{i\perp}}\,\mathrm{tr}\left(\lambda^a\,\left[\lambda^{d_0},\left[\lambda^{d_1},...,\left[\lambda^{d_{n+1}},\lambda^b\right]\right]\right]\right)\,. \end{aligned} \tag{10}$$

The configuration with all the helicities $\nu=-$ is obtained by replacing the complex conjugates of eq.(7) and (8) into eq.(2), which amounts to exchange $\prod_i p_{i\perp}$ with $\prod_i p^*_{i\perp}$ in eq.(10).

The calculation of the FKL amplitude for the other helicity configurations at the helicity-conserving vertices is obtained from the one of eq.(10), by taking the suitable complex conjugates of the contractions (8),

$$\begin{aligned} M(p_A,-;p_0,-;...;p_{n+1},+;p_B,+) &= M(p_A,+;p_0,+;...;p_{n+1},+;p_B,+)\,, && (11)\\ M(p_A,+;p_0,+;...;p_{n+1},-;p_B,-) &= M(p_A,-;p_0,-;...;p_{n+1},-;p_B,-)\,, && (12)\\ &= \left(\frac{p_{n+1\perp}}{p^*_{n+1\perp}}\right)^2 M(p_A,+;p_0,+;...;p_{n+1},+;p_B,+)\,, && \end{aligned}$$

with helicities $\nu_i = +$ and $i = 1, ..., n$. Finally, changing the helicity of a gluon along the ladder by means of eq.(7), the amplitude (10) changes only by a phase,

$$\begin{aligned} & M(p_A,+;p_0,+;...;p_{j-1},+;p_j,-;p_{j+1},+;...;p_{n+1},+;p_B,+) \qquad (13)\\ & = \frac{p_{i\perp} q_{i\perp} q^*_{i+1\perp}}{p^*_{i\perp} q^*_{i\perp} q_{i+1\perp}}\, M(p_A,+;p_0,+;...;p_{n+1},+;p_B,+)\,. \end{aligned}$$

2.2 The Parke-Taylor amplitudes in the multi-Regge kinematics

A tree-level multigluon amplitude in a helicity basis has in general the form [17]

$$M_n = \sum_{[A,0,...,n+1,B]} \mathrm{tr}(\lambda^a \lambda^{d_0} \cdots \lambda^{d_{n+1}} \lambda^b)\, m(\tilde p_A, \epsilon_A; p_0, \epsilon_0; ...; p_{n+1}, \epsilon_{n+1}; \tilde p_B, \epsilon_B)\,, \qquad (14)$$

where the sum is over the noncyclic permutations of the color orderings $[A, 0, ..., B]$. Considering all the momenta as outgoing, the PT amplitudes describe the *maximally helicity-violating* configurations $(-, -, +, ..., +)$ for which the subamplitudes, $m(\tilde p_A, \epsilon_A; p_0, \epsilon_0; ...; p_{n+1}, \epsilon_{n+1}; \tilde p_B, \epsilon_B)$, invariant with respect to tranformations between physical gauges, assume the form [6], [17][2],

$$im(-,-,+,...,+) = 2^{2+n/2}\, i\, g^{n+2} \frac{\langle p_i p_j \rangle^4}{\langle \tilde{p}_A p_0 \rangle \cdots \langle p_{n+1} \tilde{p}_B \rangle \langle \tilde{p}_B \tilde{p}_A \rangle}\,, \tag{15}$$

where i and j are the gluons of negative helicity, and the ordering of the spinor products in the denominator is set by the permutation of the color ordering $[A, 0, ..., B]$. The subamplitudes (15) are *exact*, i.e. valid for arbitrary kinematics. In eq.(15) the representation (93) (Appendix A) for the gluon polarization has been used. The configurations $(+,+,-,...,-)$ are then obtained by replacing the $\langle pk \rangle$ products with $[kp]$ products.

Computing the spinor products in eq.(15) by means of eq.(105) (Appendix B), we find that the leading color orderings in the multi-Regge kinematics are given by the 2^{n+2} configurations which respect the rapidity ordering on the two-sided lego plot in rapidity and azimuthal angle [5], [13], [14]. The second side of the lego plot is obtained by untwisting the color lines in a given color ordering. An example for the color orderings $[A, 0, ..., j-1, j+1, ..., n+1, B, j]$, with $j = 0, ..., n+1$, is given in Fig. 2. All the leading color orderings are the ones given by eq.(9). Then for the helicity configurations of eq.(10), (11) and (12), the PT amplitudes in the multi-Regge kinematics are equal to the FKL amplitudes [5].

---

[2] Note that eq.(15) differs for the $\sqrt{2}$ factors from the expression given in ref.[17], because we use the standard normalization of the λ matrices, $\mathrm{tr}(\lambda^a \lambda^b) = \delta^{ab}/2$.

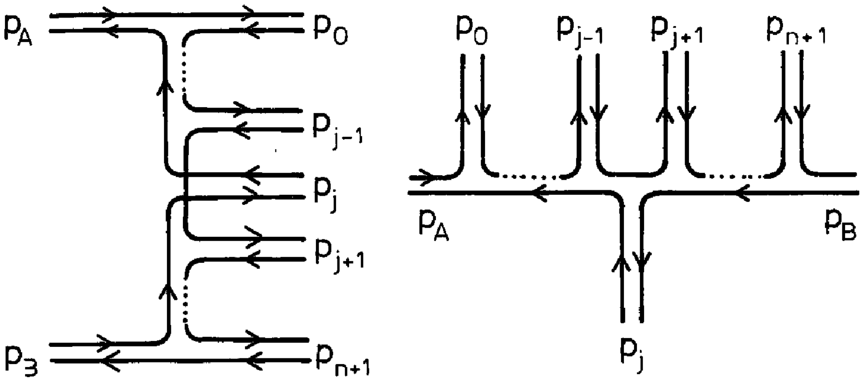

Figure 2: *a*) PT amplitude with color ordering $[A, 0, ..., j-1, j+1, ..., n+1, B, j]$, and *b*) its untwisted version on the two-sided lego plot.

3 Next-to-leading corrections in the forward-rapidity region

In order to compute the next-to-leading corrections to the FKL amplitudes in the forward-rapidity region, we consider the production of 3 gluons of momenta k_1, k_2 and p' in the scattering between two gluons of momenta k_0 and p, with gluons k_1 and k_2 in the forward-rapidity region of gluon k_0 (Fig. 3); thus we require that gluons k_1 and k_2 have likewise rapidity, but much larger than the one of p', and that they all have comparable transverse momenta,

$$y_1 \simeq y_2 \gg y' ; \qquad |k_{1\perp}| \simeq |k_{2\perp}| \simeq |p'_\perp| . \tag{16}$$

We are going to show that the amplitude for the production of 3 gluons in the helicity configuration $(-k_0, -\nu_0; k_1, \nu_1; k_2, \nu_2; p', \nu'; -p, -\nu)$ may be written as,

$$
\begin{aligned}
& i\, M(-k_0, -\nu_0; k_1, \nu_1; k_2, \nu_2; p', \nu'; -p, -\nu) \\
& = 2\sqrt{2}\, i\, g^3\, \frac{\hat{s}}{|p'_\perp|^2}\, C_{-\nu\nu'}(-p, p')\, \{A_{-\nu_0\nu_1\nu_2}(-k_0, k_1, k_2) \\
& \times \mathrm{tr}\left(\lambda^{d_0}\lambda^{d_1}\lambda^{d_2}\lambda^{d'}\lambda^{d} - \lambda^{d_0}\lambda^{d_1}\lambda^{d_2}\lambda^{d}\lambda^{d'} + \lambda^{d_0}\lambda^{d'}\lambda^{d}\lambda^{d_2}\lambda^{d_1} - \lambda^{d_0}\lambda^{d}\lambda^{d'}\lambda^{d_2}\lambda^{d_1}\right) \\
& - B_{-\nu_0\nu_1\nu_2}(-k_0, k_1, k_2)\, \mathrm{tr}\left(\lambda^{d_0}\lambda^{d_1}\lambda^{d'}\lambda^{d}\lambda^{d_2} - \lambda^{d_0}\lambda^{d_2}\lambda^{d}\lambda^{d'}\lambda^{d_1}\right) + (1 \leftrightarrow 2)\Big\}\ ,
\end{aligned}
\tag{17}
$$

with the production vertex C of gluon p' determined by the first of eq.(8),

$$
C_{-+}(-p, p') = \frac{p'^{*}_{\perp}}{p'_{\perp}} \qquad C_{+-}(-p, p') = C^{*}_{-+}(-p, p')\,, \tag{18}
$$

and with the vertices A and B computed in sect. 3.1. The following considerations motivate the analytic form of eq.(17): because of the large rapidity interval between gluons k_1 and k_2 and gluon p' we expect the amplitude to be dominated by gluon exchange in the crossed channel, and thus to scale like $\hat{s}/|p'_\perp|^2$, $-|p'_\perp|^2$ being the momentum transfer $\hat{t}$ (108) (Appendix C). In addition, we write eq.(17) in such a way to stress that the vertex C of gluon p' and the vertices A and B of gluons k_1 and k_2, which the amplitude factorizes into, transform separately into their complex conjugates under the respective helicity reversal, as the whole amplitude does under the overall helicity reversal.

3.1 The Parke-Taylor amplitudes

We fix $\tilde{p}_A = -k_0$ and $\tilde{p}_B = -p$ in eq.(14). From the spinor products (109) (Appendix C) and eq.(15) we note that the leading helicity configurations are the ones for which the

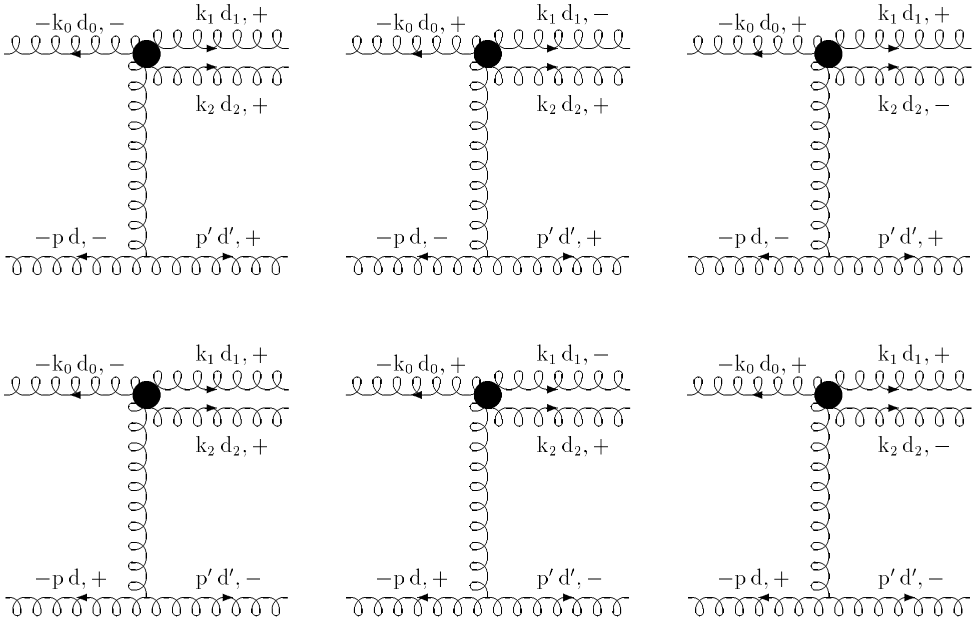

Figure 3: Leading helicity configurations of the 3-gluon production amplitude, with 2 negative-helicity gluons. The gluons are labelled by their momenta, always taken as outgoing, their colors and helicities. Gluons k_1 and k_2 are produced in the forward-rapidity region of gluon k_0.

pair of negative-helicity gluons is one of the following (Fig. 3),

$$(-p, -k_0), \quad (-p, k_i), \quad (p', -k_0), \quad (p', k_i), \tag{19}$$

with $i = 1, 2$, and to start out we consider the pair $(-p, -k_0)$ (Fig. 3a). From eq.(15) we have,

$$i\, m(-k_0, -; k_1, +; k_2, +; p', +; -p, -) = 4\sqrt{2}\, i\, g^3 \frac{\langle k_0 p\rangle^4}{\langle k_0 k_1\rangle \langle k_1 k_2\rangle \langle k_2 p'\rangle \langle p' p\rangle \langle p k_0\rangle} \,. \tag{20}$$

We insert eq.(20) back into eq.(14) and examine all the color orderings, as in ref. [5] and [14]. We start with the ordering $[0, 1, 2, p', p]$ (Fig.4a). Using the spinor products (109)

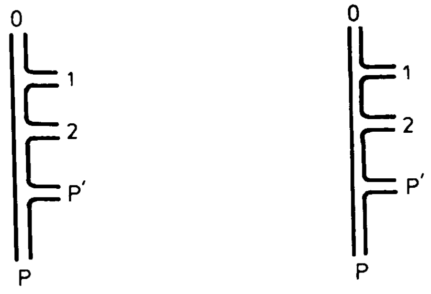

Figure 4: 3-gluon production amplitude in the color ordering (a) $[0,1,2,p',p]$ and (b) $(1 \leftrightarrow 2)$.

(Appendix C), the identity (90) (Appendix A) and eq.(18), we obtain

$$\begin{aligned} \text{coeff. of tr}\left(\lambda^{d_0}\lambda^{d_1}\lambda^{d_2}\lambda^{d'}\lambda^{d}\right) &\equiv 2\sqrt{2}\, i\, g^3 \frac{\hat{s}}{|p'_\perp|^2} C_{-+}(-p,p')\, A_{-++}(-k_0,k_1,k_2) \qquad (21) \\ A_{-++}(-k_0,k_1,k_2) &= 2\,\frac{p'_\perp}{k_{1\perp}} \frac{1}{k_{2\perp} - k_{1\perp}\frac{k_2^+}{k_1^+}}\,, \end{aligned}$$

which has a massless divergence when gluons 1 and 2 become collinear. In the multi-Regge limit, $y_1 \gg y_2$, the second term in the denominator of A_{-++} drops out, and eq.(21) is in agreement with the corresponding color ordering of eq.(10), for $n = 1$. We keep then fixed the position of gluons k_0 and p in the color ordering and permute the outgoing gluons. The contribution of the ordering $[0,2,1,p',p]$ (Fig.4b) is obtained by exchanging the labels 1 and 2 in eq.(21), however the ensuing coefficient is subleading in the multi-Regge limit, $y_1 \gg y_2$. Every other color configuration with all the gluons on the front of the lego plot is subleading to the required accuracy.

Next, we move gluon p one step to the left and consider the color orderings $[0,1,2,p,p']$ and $(1 \leftrightarrow 2)$. These correspond to untwisting the color lines as done in Fig. 2, and having gluon p' on the back of the two-sided plot (Fig.5a and 5b). Using the spinor products

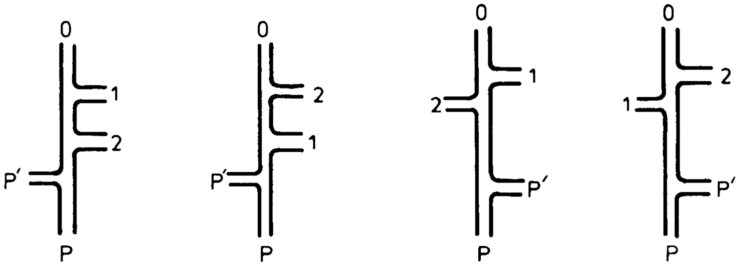

Figure 5: 3-gluon production amplitude in the color ordering (a) $[0,1,2,p,p']$ and (b) $(1 \leftrightarrow 2)$; (c) $[0,1,p',p,2]$ and (d) $(1 \leftrightarrow 2)$.

(109) (Appendix C) we find,

$$\langle k_0 k_1\rangle\langle k_1 k_2\rangle\langle k_2 p\rangle\langle p p'\rangle\langle p' k_0\rangle = -\langle k_0 k_1\rangle\langle k_1 k_2\rangle\langle k_2 p'\rangle\langle p' p\rangle\langle p k_0\rangle\,, \tag{22}$$

with the product on the right-hand side computed in eq.(21). Then we take gluon 2 to the back of the two-sided plot (Fig.5c) and consider the color ordering $[0,1,p',p,2]$. The spinor products yield,

$$\begin{aligned} \text{coeff. of tr}\left(\lambda^{d_0}\lambda^{d_1}\lambda^{d'}\lambda^{d}\lambda^{d_2}\right) &\equiv -2\sqrt{2}\,i\,g^3\,\frac{\hat{s}}{|p'_\perp|^2}\,C_{-+}(-p,p')\,B_{-++}(-k_0,k_1,k_2) \qquad (23)\\ B_{-++}(-k_0,k_1,k_2) &= 2\,\frac{p'_\perp}{k_{1\perp}k_{2\perp}}\,. \end{aligned}$$

The color ordering of eq.(23) does not contain the massless divergence when gluons 1 and 2 become collinear and is in agreement with the corresponding color ordering in the multi-Regge limit (10), for $n = 1$. The fact that the color ordering $[0,1,p',p,2]$ is finite in the collinear limit $2k_1 \cdot k_2 \to 0$, whether we compute it in the multi-Regge kinematics (1) or in the next-to-leading corrections to it (16), means that, in order to exhibit a collinear divergence, gluons 1 and 2 must be produced with equal rapidity and azimuthal angle *and* be adjacent in color space, or, in lego-plot language, that the two gluons must be overlapping on the plot *and* be produced on the same side. Finally, eq.(23) is invariant under exchange of the labels 1 and 2, thus the color ordering $[0, 2, p', p, 1]$ (Fig.5d) yields the same contribution as in eq.(23), and in particular,

$$B_{-++}(-k_0, k_1, k_2) = A_{-++}(-k_0, k_1, k_2) + A_{-++}(-k_0, k_2, k_1)\,. \tag{24}$$

The remaining two color configurations with one gluon on the back of the two-sided plot are subleading.

The other color configurations, with two or three gluons on the back of the two-sided plot, are obtained by taking the color orderings $[0, 1, 2, p', p]$, $[0, 1, 2, p, p']$, $[0, 1, p', p, 2]$, and $(1 \leftrightarrow 2)$ in reverse order. Because of the ciclicity of the traces and the identity (90) (Appendix A), this yields the same result as in eq.(21), (22) and (23) but with opposite sign.

Substituting then eq.(21-23) into eq.(14), we obtain the 3-gluon production amplitude in the helicity configuration (20) in the form of eq.(17) with C_{-+}, A_{-++} and B_{-++} given in eq.(18), (21) and (23) respectively. In the multi-Regge limit, $y_1 \gg y_2$, the 4 color configurations obtained by exchanging gluons k_1 and k_2 on the same side of the lego plot (Fig.4b and 5b and analogous ones with front and back of the lego plot exchanged) become subleading. Thus out of the 12 color configurations of eq.(17), only the 8 configurations given by eq.(9) for $n = 1$ survive, and eq.(17) is reduced to eq.(10).

Then we consider the other helicity configurations (Fig. 3b-f) in eq.(19). Substituting the product $\langle k_0 p\rangle^4$ in eq.(20) with the suitable product according to the pair of negative-helicity gluons considered, we obtain,

$$M(-k_0, +; k_1, -; k_2, +; p', +; -p, -)$$

$$= \frac{1}{\left(1+\frac{k_2^+}{k_1^+}\right)^2} M(-k_0,-;k_1,+;k_2,+;p',+;-p,-) \tag{25}$$

$$M(-k_0,-;k_1,+;k_2,+;p',-;-p,+)$$

$$= \left(\frac{p'_\perp}{p'^*_\perp}\right)^2 M(-k_0,-;k_1,+;k_2,+;p',+;-p,-) \tag{26}$$

$$M(-k_0,+;k_1,-;k_2,+;p',-;-p,+)$$

$$= \left(\frac{p'_\perp}{p'^*_\perp}\right)^2 M(-k_0,+;k_1,-;k_2,+;p',+;-p,-)\,. \tag{27}$$

In the multi-Regge limit, $y_1 \gg y_2$, eq.(25) (Fig. 3b) agrees with eq.(11). Eq.(26) (Fig. 3d) is already in agreement with its multi-Regge limit, eq.(12), since the amplitude factorizes and the lower vertex is insensitive to the next-to-leading corrections in the upper vertex. Eq.(27) (Fig. 3e) is obtained combining the results of eq.(25) and eq.(26), and in the multi-Regge limit is reduced to eq.(12). The configurations $(-k_0,+;k_1,+;k_2,-;p',+;-p,-)$ (Fig. 3c) and $(-k_0,+;k_1,+;k_2,-;p',-;-p,+)$ (Fig. 3f) are obtained by exchanging the labels 1 and 2 in eq.(25) and (27) respectively; however, in the multi-Regge limit $y_1 \gg y_2$, they are subleading since then helicity is not conserved in the production vertex of gluon k_1. Thus, 4 out of the 6 helicity configurations of eq.(19) survive in the multi-Regge limit, in agreement with ref. [5].

The configurations with only two positive-helicity gluons, which correspond to inverting the helicity of all the gluons in Fig. 3, are obtained from the ones of eq.(19) by replacing the $\langle pk\rangle$ products with $[kp]$ products, and by using eq.(91) (Appendix A). Thus they may be computed by taking the complex conjugate of the spinor products (21), (22) and (23), and by using eq.(25), (26) and (27). Added to the 6 helicity configurations (19), they cover all the 12 leading helicity configurations of the 3-gluon amplitude in the kinematics (16). In particular we consider two examples: the configuration $(-k_0,+;k_1,-;k_2,-;p',+;-p,-)$ (Fig. 6a), which corresponds to reversing all the helicities in the production vertex of gluons k_1 and k_2 (Fig. 3a), and is obtained by taking the complex conjugate of the spinor products in eq.(26). The amplitude then assumes the form of eq.(17), with $A_{+--}(-k_0,k_1,k_2) = A^*_{-++}(-k_0,k_1,k_2)$ and $B_{+--}(-k_0,k_1,k_2) = B^*_{-++}(-k_0,k_1,k_2)$, in agreement with the discussion following eq.(17); the configuration $(-k_0,-;k_1,+;k_2,-;p',+;-p,-)$ (Fig. 6b), which corresponds to reversing the helicity of one of the outgoing gluons in the upper vertex (Fig. 3a), and is obtained by taking the complex conjugate of the spinor products in eq.(27). The amplitude has the form of eq.(17), with $A_{-+-}(-k_0,k_1,k_2) = A^*_{+-+}(-k_0,k_1,k_2)$ and $B_{-+-}(-k_0,k_1,k_2) = B^*_{+-+}(-k_0,k_1,k_2)$ and $A_{+-+}(-k_0,k_1,k_2)$ and $B_{+-+}(-k_0,k_1,k_2)$ defined by eq.(25). By taking then the multi-Regge limit of eq.(17) with $(\nu_0\nu_1\nu_2) = (-+-)$ and $(\nu_0\nu_1\nu_2) = (-++)$ we obtain,

$$\begin{aligned} &\lim_{y_1\gg y_2} M(-k_0,-;k_1,+;k_2,-;p',+;-p,-) \\ &= \frac{p'^*_\perp k_{1\perp} k_{2\perp}}{p'_\perp k^*_{1\perp} k^*_{2\perp}} \lim_{y_1\gg y_2} M(-k_0,-;k_1,+;k_2,+;p',+;-p,-)\,, \end{aligned} \tag{28}$$

in agreement with the helicity flip in the Lipatov vertex of gluon k_2 in the FKL amplitudes, eq.(13), with $q_{1\perp} \equiv -k_{1\perp}$, $q_{2\perp} \equiv p'_\perp$ and $p_{1\perp} \equiv k_{2\perp}$.

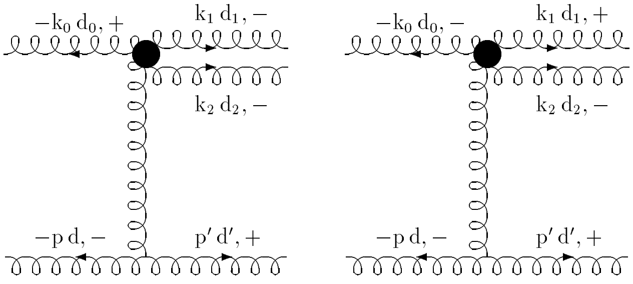

Figure 6: 3-gluon production amplitude, with 2 positive-helicity gluons.

The extension of the kinematics (16) to the production of $n+2$ gluons, with 2 gluons with likewise rapidity in the forward-rapidity region of the upper vertex (111-113) (Appendix C), is straightforward. Generalizing equations (21-23) to the production of $n+2$ gluons and using them to compute the other color configurations, the amplitude for the extension of the helicity configuration of Fig. 3a is,

$$\begin{aligned}
& i\,M(-k_0,-;k_1,+;k_2,+;p_1,+;...;p_n,+;-p,-) \\
& = (-1)^{n+1}\,2^{2+n/2}\,i\,g^{n+2}\,\hat{s}\,\frac{1}{\prod_{i=1}^{n} p_{i\perp}} \Biggl\{ \Biggl[\frac{1}{k_{1\perp}} \frac{1}{k_{2\perp} - k_{1\perp}\frac{k_2^+}{k_1^+}} \\
& \times \mathrm{tr}\Biggl(\lambda^{d_0}\lambda^{d_1}\lambda^{d_2}\lambda^{p_1}\cdots\lambda^{p_n}\lambda^{p} - \sum_{i=1}^{n} \lambda^{d_0}\lambda^{d_1}\lambda^{d_2}\lambda^{p_1}\cdots\lambda^{p_{i-1}}\lambda^{p_{i+1}}\cdots\lambda^{p_n}\lambda^{p}\lambda^{p_i} \\
& + \lambda^{d_0}\lambda^{p_1}\cdots\lambda^{p_n}\lambda^{p}\lambda^{d_2}\lambda^{d_1} + \sum_{i<j} \lambda^{d_0}\lambda^{d_1}\lambda^{d_2}\lambda^{p_1}\cdots\lambda^{p_{i-1}}\lambda^{p_{i+1}}\cdots\lambda^{p_{j-1}}\lambda^{p_{j+1}}\cdots\lambda^{p_n}\lambda^{p}\lambda^{p_j}\lambda^{p_i} + ... \Biggr) \\
& - \frac{1}{k_{1\perp}k_{2\perp}} \mathrm{tr}\Biggl(\lambda^{d_0}\lambda^{d_1}\lambda^{p_1}\cdots\lambda^{p_n}\lambda^{p}\lambda^{d_2} - \sum_{i=1}^{n} \lambda^{d_0}\lambda^{d_1}\lambda^{p_1}\cdots\lambda^{p_{i-1}}\lambda^{p_{i+1}}\cdots\lambda^{p_n}\lambda^{p}\lambda^{p_i}\lambda^{d_2} + ... \Biggr) \Biggr] \\
& + (1 \leftrightarrow 2) \Biggr\} \,,
\end{aligned} \tag{29}$$

where we have explicitly shown the color configurations with $n+2$, $n+1$ and n gluons on the front of the lego plot. By explicit counting, we see that the leading color configurations in eq.(29) are $3!\,2^n$, which for $n=1$ yields the 12 color configurations of eq.(17). The other helicity configurations with 2 negative or 2 positive-helicity gluons may be accordingly generalized.

3.2 The Fadin-Lipatov amplitudes

The 3-gluon production amplitude, with gluons k_1 and k_2 produced in the forward-rapidity region of gluon k_0, as specified by the kinematics (16), has been computed in ref. [9], and for a generic helicity configuration is given by,

$$\begin{aligned} & i\, M^{d_0 d_1 d_2 d' d}_{\nu_0 \nu_1 \nu_2 \nu' \nu} = \epsilon^{\nu_0 *}_{\mu_0}(k_0)\epsilon^{\nu_1}_{\mu_1}(k_1)\epsilon^{\nu_2}_{\mu_2}(k_2)\epsilon^{\nu *}_{\mu}(p)\epsilon^{\nu'}_{\mu'}(p')\, 4\, g^3\, \frac{1}{\hat{t}} f^{d' c d}\Gamma^{\mu\mu'}(p,p',-k_0) \\ & \times \Big\{ \Gamma^{\mu_0 \mu_1}(-k_0,k_1,p) \Big[f^{d_0 c' d_2} f^{d_1 c' c} D^{\mu_2}(-k_0,k_1,k_2) + f^{d_0 c' c} f^{d_1 c' d_2} D^{\mu_2}(k_1,-k_0,k_2) \Big] \\ & + \begin{pmatrix} k_1 \leftrightarrow k_2 \\ \nu_1 \leftrightarrow \nu_2 \\ d_1 \leftrightarrow d_2 \end{pmatrix} + \begin{pmatrix} -k_0 \leftrightarrow k_2 \\ \nu_0 \leftrightarrow \nu_2 \\ d_0 \leftrightarrow d_2 \end{pmatrix} \Big\} \,, \end{aligned} \tag{30}$$

where the Γ-tensors are given in eq.(3), and the 2-gluon production vertex D in the forward-rapidity region is [9],

$$\begin{aligned} & D^{\mu}(k_0,k_1,k_2) \\ & = \frac{1}{k_0 \cdot k_1} \left[\left(k_1 \cdot k_2 - p \cdot p' \frac{k_1 \cdot p}{k_2 \cdot p} \right) p^{\mu} + \frac{k_1 \cdot p}{k_0 \cdot k_2} (k_1 \cdot k_2 + p \cdot p')\, k_0^{\mu} + k_0 \cdot p\, k_1^{\mu} \right] \,, \end{aligned} \tag{31}$$

with the Mandelstam invariants given in eq.(108) (Appendix C). The D-vertex is gauge invariant with respect to the last of its arguments,

$$D(-k_0,k_1,k_2) \cdot k_2 = 0 \,, \tag{32}$$

where we have used the + momentum conservation (107) (Appendix C). Using eq.(32) and the gauge invariance of the Γ-tensors (5), one can see that the amplitude (30) is invariant with respect to arbitrary gauge transformations [9], [18]. The symmetry of the amplitude (30) under permutations of the gluons in the forward-rapidity region is manifest.

In order to make the color structure explicit, we use eq.(9) and rewrite eq.(30) as

$$\begin{aligned} & i\, M^{d_0 d_1 d_2 d' d}_{\nu_0 \nu_1 \nu_2 \nu' \nu} = -\epsilon^{\nu_0 *}_{\mu_0}(k_0)\epsilon^{\nu_1}_{\mu_1}(k_1)\epsilon^{\nu_2}_{\mu_2}(k_2)\epsilon^{\nu *}_{\mu}(p)\epsilon^{\nu'}_{\mu'}(p')\, 8\, (-i)^3\, g^3\, \frac{1}{\hat{t}} \Gamma^{\mu\mu'}(p,p',-k_0) \\ & \times \{ [\Gamma^{\mu_0 \mu_1}(-k_0,k_1,p) D^{\mu_2}(-k_0,k_1,k_2) - \Gamma^{\mu_2 \mu_1}(k_2,k_1,p) D^{\mu_0}(k_2,k_1,-k_0)] \end{aligned}$$

$$
\begin{aligned}
&\times \mathrm{tr}\left(\lambda^{d_0}\,\left[\lambda^{d_2},\left[\lambda^{d_1},\left[\lambda^{d'},\lambda^{d}\right]\right]\right]\right) \\
&+\left[\Gamma^{\mu_0\mu_1}(-k_0,k_1,p)D^{\mu_2}(k_1,-k_0,k_2)-\Gamma^{\mu_0\mu_2}(-k_0,k_2,p)D^{\mu_1}(k_2,-k_0,k_1)\right] \\
&\times \mathrm{tr}\left(\lambda^{d_1}\,\left[\lambda^{d_2},\left[\lambda^{d_0},\left[\lambda^{d'},\lambda^{d}\right]\right]\right]\right) \\
&+\left[\Gamma^{\mu_0\mu_2}(-k_0,k_2,p)D^{\mu_1}(-k_0,k_2,k_1)-\Gamma^{\mu_2\mu_1}(k_2,k_1,p)D^{\mu_0}(k_1,k_2,-k_0)\right] \\
&\times \mathrm{tr}\left(\lambda^{d_0}\,\left[\lambda^{d_1},\left[\lambda^{d_2},\left[\lambda^{d'},\lambda^{d}\right]\right]\right]\right)\Big\}\,. \qquad (33)
\end{aligned}
$$

Eq.(33) simplifies considerably once the gluon helicities are fixed. For sake of comparison with the PT amplitudes, we consider the configuration with helicities $\nu_0=\nu_1=\nu_2=+$. We perform the contractions of the helicity-conserving tensors (3) with the gluon polarizations using eq.(110) (Appendix C). For the incoming gluons they of course coincide with eq.(8),

$$
\begin{aligned}
\Gamma^{\mu\mu'}(p,p',-k_0)\,\epsilon^{+*}_{\mu}(p,k_0)\,\epsilon^{+}_{\mu'}(p',k_0) &= -\frac{p'^{*}_{\perp}}{p'_{\perp}} \\
\Gamma^{\mu_0\mu_i}(-k_0,k_i,p)\,\epsilon^{+*}_{\mu_0}(k_0,p)\,\epsilon^{+}_{\mu_i}(k_i,p) &= -1 \qquad (34) \\
\Gamma^{\mu_2\mu_1}(k_2,k_1,p)\,\epsilon^{+}_{\mu_2}(k_2,p)\,\epsilon^{+}_{\mu_1}(k_1,p) &= 0\,,
\end{aligned}
$$

with $i=1,2$. Accordingly, eq.(33) becomes

$$
\begin{aligned}
&i\,M(k_0,+;k_1,+;k_2,+;p',\nu';p,\nu) = -8\,(-i)^3\,g^3\,\frac{1}{\hat{t}}\,C_{\nu\nu'}(p,p') \\
&\times\Big\{D(-k_0,k_1,k_2)\cdot\epsilon^{+}(k_2,p)\,\mathrm{tr}\left(\lambda^{d_0}\,\left[\lambda^{d_2},\left[\lambda^{d_1},\left[\lambda^{d'},\lambda^{d}\right]\right]\right]\right) \qquad (35) \\
&+\Big[D(k_1,-k_0,k_2)\cdot\epsilon^{+}(k_2,p)\;-D(k_2,-k_0,k_1)\cdot\epsilon^{+}(k_1,p)\Big]\,\mathrm{tr}\left(\lambda^{d_1}\,\left[\lambda^{d_2},\left[\lambda^{d_0},\left[\lambda^{d'},\lambda^{d}\right]\right]\right]\right) \\
&+D(-k_0,k_2,k_1)\cdot\epsilon^{+}(k_1,p)\mathrm{tr}\left(\lambda^{d_0}\,\left[\lambda^{d_1},\left[\lambda^{d_2},\left[\lambda^{d'},\lambda^{d}\right]\right]\right]\right)\Big\}\,,
\end{aligned}
$$

with the C-vertex defined like in eq.(18),

$$
C_{++}(p,p')=\frac{p'^{*}_{\perp}}{p'_{\perp}} \qquad C_{--}(p,p')=C^{*}_{++}(p,p')\,. \qquad (36)
$$

Using eq.(9), we unfold the nested commutators in eq.(35), where it is convenient to rewrite the second as,

$$\mathrm{tr}\left(\lambda^{d_1}\,\left[\lambda^{d_2},\left[\lambda^{d_0},\left[\lambda^{d'},\lambda^{d}\right]\right]\right]\right)=\mathrm{tr}\left(\lambda^{d_0}\,\left[\left[\lambda^{d_2},\lambda^{d_1}\right],\left[\lambda^{d'},\lambda^{d}\right]\right]\right)\,. \tag{37}$$

The color orderings we obtain are the same as in eq.(17), and we compute their coefficients starting with the one of $\mathrm{tr}\left(\lambda^{d_0}\lambda^{d_1}\lambda^{d_2}\lambda^{d'}\lambda^{d}\right)$. Performing the contractions of the D-vertices (31) with the gluon polarizations (110) (Appendix C), we obtain, after some algebraic manipulations,

$$\begin{aligned}&\text{coeff. of tr}\left(\lambda^{d_0}\lambda^{d_1}\lambda^{d_2}\lambda^{d'}\lambda^{d}\right)=-8\,(-i)^3\,g^3\,\frac{1}{\hat{t}}\,C_{\nu\nu'}(p,p')\\&\times\Big[D(-k_0,k_2,k_1)\cdot\epsilon^+(k_1,p)-D(k_1,-k_0,k_2)\cdot\epsilon^+(k_2,p)+D(k_2,-k_0,k_1)\cdot\epsilon^+(k_1,p)\Big]\\&=4\sqrt{2}i\,g^3\,\frac{\hat{s}}{|p'_\perp|^2}C_{\nu\nu'}(p,p')\,\frac{p'_\perp}{k_{1\perp}}\frac{1}{k_{2\perp}-k_{1\perp}\frac{k_2^+}{k_1^+}}\,.\end{aligned} \tag{38}$$

In addition, eq.(35) is manifestly antisymmetric under the exchange $d\leftrightarrow d'$, thus

$$\text{coeff. of tr}\left(\lambda^{d_0}\lambda^{d_1}\lambda^{d_2}\lambda^{d}\lambda^{d'}\right)=-\text{coeff. of tr}\left(\lambda^{d_0}\lambda^{d_1}\lambda^{d_2}\lambda^{d'}\lambda^{d}\right)\,, \tag{39}$$

plus contributions with the labels of gluons 1 and 2 exchanged in eq.(38) and (39). The coefficient of $\mathrm{tr}\left(\lambda^{d_0}\lambda^{d_1}\lambda^{d'}\lambda^{d}\lambda^{d_2}\right)$ is symmetric under the exchange of gluons 1 and 2,

$$\begin{aligned}&\text{coeff. of tr}\left(\lambda^{d_0}\lambda^{d_1}\lambda^{d'}\lambda^{d}\lambda^{d_2}\right)\\&=8\,(-i)^3\,g^3\,\frac{1}{\hat{t}}\,C_{\nu\nu'}(p,p')\,\Big[D(-k_0,k_1,k_2)\cdot\epsilon^+(k_2,p)+D(-k_0,k_2,k_1)\cdot\epsilon^+(k_1,p)\Big]\\&=-4\sqrt{2}\,i\,g^3\,\frac{\hat{s}}{|p'_\perp|^2}C_{\nu\nu'}(p,p')\,\frac{p'_\perp}{k_{1\perp}k_{2\perp}}\,.\end{aligned} \tag{40}$$

The contraction,

$$D(-k_0,k_1,k_2)\cdot\epsilon^+(k_2,p)=-\frac{k_0\cdot p}{\sqrt{2}}\left(\frac{k_{1\perp}^*}{k_0\cdot k_1}+\frac{k_{2\perp}^*}{k_0\cdot k_2}\frac{k_1^+}{k_2^+}\right) \tag{41}$$

used in eq.(40), is proportional in the multi-Regge limit to the Lipatov vertex,

$$\begin{aligned}\lim_{y_1 \gg y_2} D(-k_0, k_1, k_2) \cdot \epsilon^+(k_2, p) &= \frac{1}{\sqrt{2}} \frac{k_0 \cdot p}{k_0 \cdot k_1} \frac{k^*_{1\perp} p'_\perp}{k_{2\perp}} \\ &= -\frac{1}{2} \frac{k_0 \cdot p}{k_0 \cdot k_1} \epsilon^+(k_2, p) \cdot C(q_1, q_2)\,,\end{aligned} \tag{42}$$

in agreement with ref. [9]. In eq.(42) we have used the multi-Regge limit (104) (Appendix B) of the invariants (108) (Appendix C), and eq.(7) with $q_{1\perp} \equiv -k_{1\perp}$, $q_{2\perp} \equiv p'_\perp$ and $p_{1\perp} \equiv k_{2\perp}$.

In the two-sided lego-plot picture, $\mathrm{tr}\left(\lambda^{d_0} \lambda^{d_1} \lambda^{d_2} \lambda^{d'} \lambda^{d}\right)$ plus $(1 \leftrightarrow 2)$, yields the leading color configurations with all the gluons on the front of the lego plot (Fig.4); $\mathrm{tr}\left(\lambda^{d_0} \lambda^{d_1} \lambda^{d_2} \lambda^{d} \lambda^{d'}\right)$ and $\mathrm{tr}\left(\lambda^{d_0} \lambda^{d_1} \lambda^{d'} \lambda^{d} \lambda^{d_2}\right)$ plus $(1 \leftrightarrow 2)$, yield the leading color configurations with one gluon on the back of the lego plot (Fig.5). The coefficients of the color configurations with two and three gluons on the back of the lego plot are obtained by changing the sign to the ones with three gluons (38) and two gluons (39), (40) on the front of the lego plot, as can be seen by direct inspection of the unfolded nested commutators in eq.(35). Thus, using eq.(38-40), eq.(35) is reduced to eq.(17), proving the equivalence of the Fadin-Lipatov and the helicity amplitudes for the configuration of eq.(20). Analogously all the other leading helicity configurations may be computed from eq.(33), and compared to the helicity amplitudes of sect. 3.1.

4 Next-to-leading corrections in the central-rapidity region

In order to compute the next-to-leading corrections to the FKL amplitudes in the central-rapidity region, we consider the production of 4 gluons of momenta p'_A, k_1, k_2 and p'_B in the scattering between two gluons of momenta p_A and p_B. We require that gluons k_1 and k_2 have likewise rapidity and are separated through large rapidity intervals from the forward-rapidity regions, with all the gluons having comparable transverse momenta,

$$y'_A \gg y_1 \simeq y_2 \gg y'_B \, ; \qquad |k_{1\perp}| \simeq |k_{2\perp}| \simeq |p'_{A\perp}| \simeq |p'_{B\perp}| \, . \tag{43}$$

We are going to show that the amplitude for the production of 4 gluons in the helicity configuration $(-p_A, -\nu_A; p'_A, \nu'_A; k_1, \nu_1; k_2, \nu_2; p'_B, \nu'_B; -p_B, -\nu_B)$ has the form,

$$\begin{aligned}
& i\, M(-p_A, -\nu_A; p'_A, \nu'_A; k_1, \nu_1; k_2, \nu_2; p'_B, \nu'_B; -p_B, -\nu_B) \qquad (44)\\
&= -4\, i\, g^4 \, \frac{\hat{s}}{|p'_{A\perp}|^2 |p'_{B\perp}|^2} \, C_{-\nu_A \nu'_A}(-p_A, p'_A) \, C_{-\nu_B \nu'_B}(-p_B, p'_B) \\
&\times \Big\{ A_{\nu_1\nu_2}(k_1,k_2) \, \Big[\mathrm{tr} \left(\lambda^a \lambda^{a'} \lambda^{d_1} \lambda^{d_2} \lambda^{b'} \lambda^b - \lambda^a \lambda^{a'} \lambda^{d_1} \lambda^{d_2} \lambda^b \lambda^{b'} \right.\\
&\left. - \lambda^a \lambda^{d_1} \lambda^{d_2} \lambda^{b'} \lambda^b \lambda^{a'} + \lambda^a \lambda^{d_1} \lambda^{d_2} \lambda^b \lambda^{b'} \lambda^{a'} \right) + \mathrm{traces\, in\, reverse\, order} \Big] - B_{\nu_1\nu_2}(k_1,k_2) \\
&\times \Big[\mathrm{tr} \left(\lambda^a \lambda^{a'} \lambda^{d_1} \lambda^{b'} \lambda^b \lambda^{d_2} - \lambda^a \lambda^{a'} \lambda^{d_1} \lambda^b \lambda^{b'} \lambda^{d_2} \right) + \mathrm{traces\, in\, reverse\, order} \Big] + (1 \leftrightarrow 2)_{\nu_1/\nu_2} \Big\} \, ,
\end{aligned}$$

with the production vertices C of gluons p'_A and p'_B determined by eq.(8),

$$\begin{aligned}
C_{-+}(-p_A, p'_A) &= C_{+-}(-p_A, p'_A) = 1 \\
C_{-+}(-p_B, p'_B) &= \frac{p'^*_{B\perp}}{p'_{B\perp}} \qquad C_{+-}(-p_B, p'_B) = C^*_{-+}(-p_B, p'_B) \, ,
\end{aligned} \tag{45}$$

and with $A_{\nu_1\nu_2}(k_1,k_2)$ and $B_{\nu_1\nu_2}(k_1,k_2)$ computed in sect. 4.1 and 4.2. In addition,

$$(1 \leftrightarrow 2)_{\nu_1/\nu_2} = \left\{ \begin{array}{ll} (1 \leftrightarrow 2) & \mathrm{for} \quad \nu_1 = \nu_2 = \pm \\ (1 \leftrightarrow 2)\, \mathcal{C} & \mathrm{for} \quad \nu_1 = -\nu_2 = \pm, \end{array} \right. \tag{46}$$

with $\mathcal{C}$ the complex conjugation. As in eq.(17) we stress that the two vertices for the production of gluons p'_A and p'_B in the forward-rapidity regions, and the vertices of gluons k_1 and k_2 in the central-rapidity region transform separately under the respective helicity reversal. However, differently from eq.(17) we note that in eq.(44) the color structure is linked through eq.(46) to the helicity structure. This is due to the fact that besides the PT amplitudes, which describe the production of gluons k_1 and k_2 with equal helicities (sect. 4.1), and for which the color and the helicity structures are uncorrelated, we use, in order to consider the production of gluons k_1 and k_2 with opposite helicities, the amplitudes with 3 negative-helicity gluons (sect. 4.2), for which the color and the helicity structures are intertwined.

4.1 The Parke-Taylor amplitudes

We fix $\tilde{p}_A = -p_A$ and $\tilde{p}_B = -p_B$ in eq.(14). From the spinor products (117) (Appendix D) and eq.(15), the leading helicity configurations are the same as in the multi-Regge kinematics (Fig. 7a-d) [5], i.e. the ones for which the pair of negative-helicity gluons is one of the following,

$$(-p_A, -p_B), \quad (-p_A, p'_B), \quad (-p_B, p'_A), \quad (p'_A, p'_B)\,. \tag{47}$$

As usual, we start with the pair $(-p_A, -p_B)$ (Fig. 7a). From eq.(15) we have,

$$\begin{aligned} & i\, m(-p_A, -; p'_A, +; k_1, +; k_2, +; p'_B, +; -p_B, -) \\ & = 8\, i\, g^4 \frac{\langle p_A p_B\rangle^4}{\langle p_A p'_A\rangle \langle p'_A k_1\rangle \langle k_1 k_2\rangle \langle k_2 p'_B\rangle \langle p'_B p_B\rangle \langle p_B p_A\rangle}\,. \end{aligned} \tag{48}$$

We insert eq.(48) into eq.(14) and examine all the color orderings, starting with

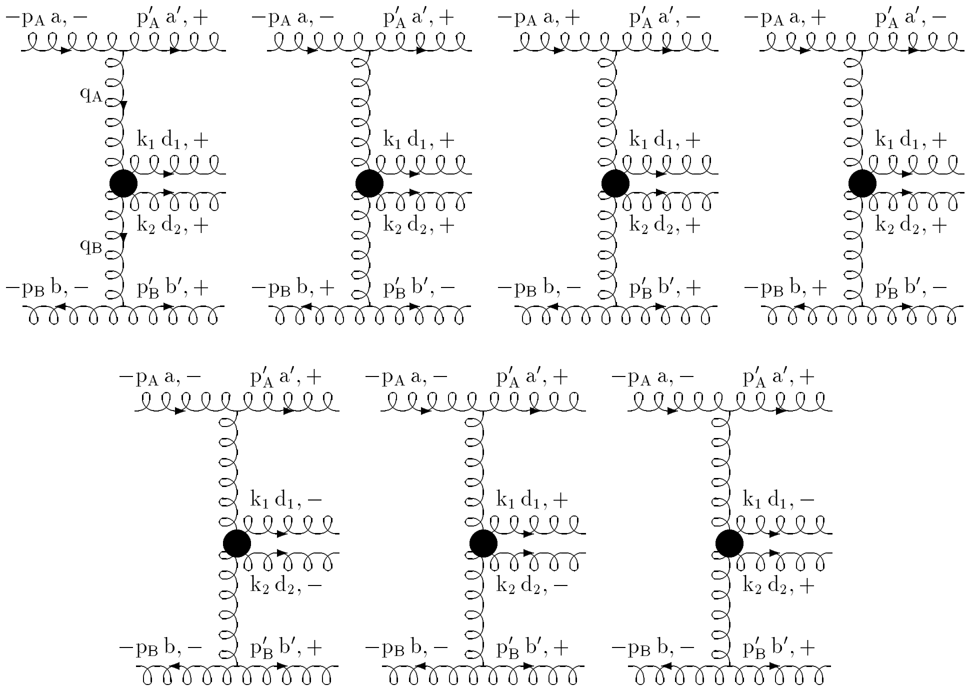

Figure 7: 4-gluon production amplitude, with 2 gluons with likewise rapidity in the central region; $(a-d)$ leading helicity configurations with 2 negative-helicity gluons; $(e-g)$ helicity reversal in the production vertex of gluons k_1 and k_2, with respect to the configuration a.

$[A, A', 1, 2, B', B]$ (Fig. 8a) and $(1 \leftrightarrow 2)$ (Fig.8b). Using the spinor products (117) (Appendix D) and eq.(45), we obtain

$$\begin{aligned}
\text{coeff. of tr}\left(\lambda^a\lambda^{a'}\lambda^{d_1}\lambda^{d_2}\lambda^{b'}\lambda^b\right) &\equiv -4\,i\,g^4\,\frac{\hat{s}}{|p'_{A\perp}|^2|p'_{B\perp}|^2}C_{-+}(-p_B,p'_B)A_{++}(k_1,k_2)\\
A_{++}(k_1,k_2) &= 2\,\frac{p'^{*}_{A\perp}p'_{B\perp}}{k_{1\perp}}\frac{1}{k_{2\perp}-k_{1\perp}\frac{k_2^+}{k_1^+}}\,,
\end{aligned} \tag{49}$$

which has a massless divergence when gluons 1 and 2 become collinear. As expected, the result is analogous to the one of eq.(21), given the similarity of the color and the helicity structures. The multi-Regge limit, $y_1 \gg y_2$, of eq.(49) is in agreement with

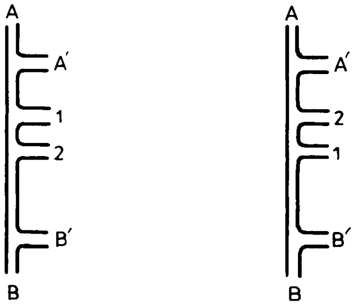

Figure 8: 4-gluon production amplitude in the color orderings $[A, A', 1, 2, B', B]$ and $(1 \leftrightarrow 2)$.

the corresponding color ordering of eq.(10), for $n = 2$. We keep then fixed the position of gluons A and B in the color ordering and permute the outgoing gluons. The same considerations made after eq.(21) apply here, namely the contribution of the ordering $[A, A', 2, 1, B', B]$ (Fig.8b) is obtained by exchanging the labels 1 and 2 in eq.(49), however the ensuing coefficient is subleading in the multi-Regge limit, $y_1 \gg y_2$. Every other color configuration with all the gluons on the front of the lego plot is subleading to the required accuracy.

Then we move gluon B one step to the left and consider the color orderings $[A, A', 1, 2, B, B']$ and $[A, 1, 2, B', B, A']$, and $(1 \leftrightarrow 2)$. These correspond respectively to have gluons B' or A' on the back of the lego plot (Fig.9a, b, c, d); the respective strings of spinor products may be related to eq.(49) through,

$$\langle p'_A k_1\rangle\langle k_2 p_B\rangle\langle p'_B p_A\rangle = \langle p_A k_1\rangle\langle k_2 p'_B\rangle\langle p_B p'_A\rangle = \langle p'_A k_1\rangle\langle k_2 p'_B\rangle\langle p_B p_A\rangle\,, \qquad (50)$$

and the identity (90) (Appendix A). It turns out that the coefficients of the color orderings of Fig.9a,c are equal to eq.(49) but with opposite sign. Then we take gluon 2 to the back of the two-sided plot (Fig. 9e) and consider the color ordering $[A, A', 1, B', B, 2]$.

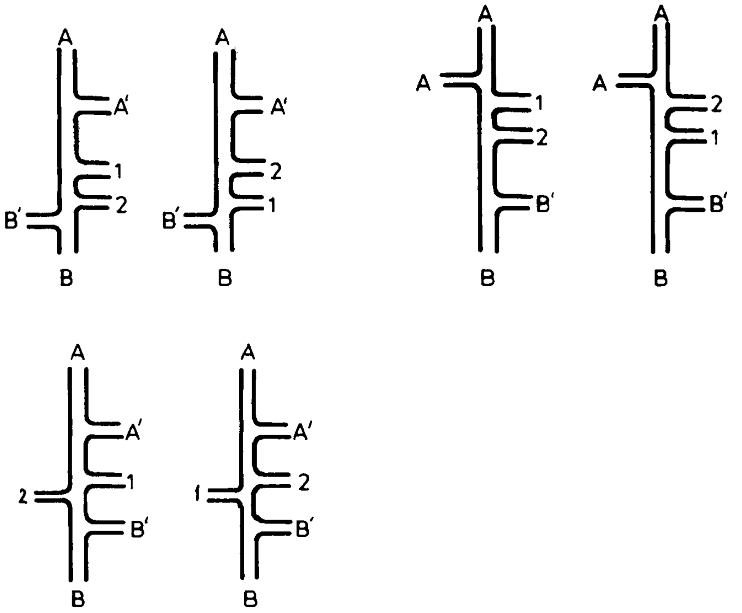

Figure 9: 4-gluon production amplitude in the color orderings (a) $[A, A', 1, 2, B, B']$ and (b) $(1 \leftrightarrow 2)$; (c) $[A, 1, 2, B', B, A']$ and (d) $(1 \leftrightarrow 2)$; (e) $[A, A', 1, B', B, 2]$ and (f) $(1 \leftrightarrow 2)$.

Similarly to eq.(23), the spinor products yield,

$$\begin{aligned} \text{coeff. of tr}\left(\lambda^a\lambda^{a'}\lambda^{d_1}\lambda^{b'}\lambda^b\lambda^{d_2}\right) &\equiv 4\,i\,g^4\,\frac{\hat{s}}{|p'_{A\perp}|^2|p'_{B\perp}|^2}\,C_{-+}(-p_B, p'_B)\,B_{++}(k_1,k_2) \\ B_{++}(k_1,k_2) &= 2\,\frac{p'^{*}_{A\perp}p'_{B\perp}}{k_{1\perp}k_{2\perp}}\,. \end{aligned} \tag{51}$$

Again, the same considerations made after eq.(23) apply here, namely eq.(51) has no massless divergence when gluons 1 and 2 become collinear; it is already in agreement with the corresponding color ordering in the multi-Regge limit (10), for $n = 2$; it is invariant under the exchange of gluons 1 and 2, thus the color ordering $[A, A', 2, B', B, 1]$ (Fig.9f) yields the same contribution as in eq.(51), and in particular,

$$B_{++}(k_1,k_2) = A_{++}(k_1,k_2) + A_{++}(k_2,k_1)\,. \tag{52}$$

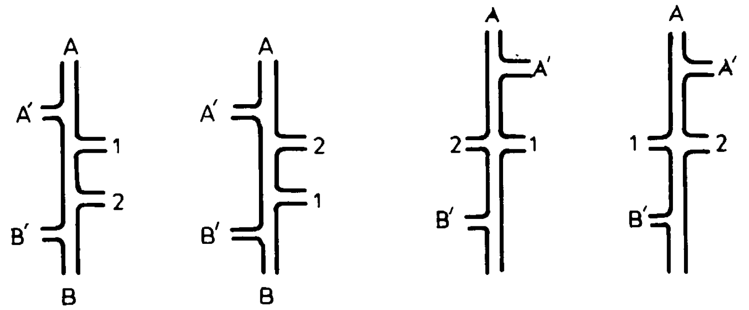

Figure 10: 4-gluon production amplitude in the color orderings (a) $[A,1,2,B,B',A']$ and (b) $(1 \leftrightarrow 2)$; (c) $[A,A',1,B,B',2]$ and (d) $(1 \leftrightarrow 2)$.

Then we move gluon B one more step to the left, in order to have two gluons on the front and two on the back of the lego plot, and consider the color ordering $[A,1,2,B,B',A']$ (Fig. 10a) and $(1 \leftrightarrow 2)$ (Fig. 10b), for which the string of spinor products may be related to eq.(49) through,

$$\langle p_A k_1\rangle\langle k_2 p_B\rangle\langle p'_B p'_A\rangle = \langle p'_A k_1\rangle\langle k_2 p'_B\rangle\langle p_B p_A\rangle\,. \tag{53}$$

The color orderings $[A,A',1,B,B',2]$ (Fig. 10c) and $(1 \leftrightarrow 2)$ (Fig. 10d), are then obtained from eq.(51), noticing that

$$\langle k_1 p_B\rangle\langle p_B p'_B\rangle\langle p'_B k_2\rangle = -\langle k_1 p'_B\rangle\langle p'_B p_B\rangle\langle p_B k_2\rangle\,. \tag{54}$$

The other color orderings with two gluons on the front and two on the back of the lego plot are obtained by taking the color orderings $[A,1,2,B,B',A']$, $[A,A',1,B,B',2]$ and $(1 \leftrightarrow 2)$ in reverse order, and by using the ciclicity of the traces and the identity (90) (Appendix A), which yields the same result as in eq.(53) and (54). Analogously, the color orderings with three or four gluons on the back of the lego plot are obtained by taking the color orderings $[A,A',1,2,B',B]$, $[A,A',1,2,B,B']$, $[A,1,2,B',B,A']$, $[A,A',1,B',B,2]$

and $(1 \leftrightarrow 2)$ in reverse order.

Substituting then equations (49-54), multiplied by the appropriate color orderings of eq.(14), we obtain the 4-gluon production amplitude in the helicity configuration (48) in the form of eq.(44), with $C_{-+}(-p_A, p'_A)$, $C_{-+}(-p_B, p'_B)$, $A_{++}(k_1, k_2)$ and $B_{++}(k_1, k_2)$ given in eq.(45), (49) and (51). In the multi-Regge limit, $y_1 \gg y_2$, the 8 color configurations obtained by exchanging gluons k_1 and k_2 on the same side of the lego plot (Fig.8b, 9b, 9d, 10b and analogous with front and back of the lego plot exchanged) become subleading. Thus out of the 24 color configurations of eq.(44), only the 16 configurations given by eq.(9) for $n = 2$ survive, and eq.(44) is reduced to eq.(10).

The other helicity configurations of eq.(47) (Fig. 7b, c, d) are obtained from eq.(48), by substituting the product $\langle p_A p_B \rangle^4$ with the suitable product according to the pair of negative-helicity gluons considered. This entails to take the suitable complex conjugates of the C-vertices (45), and the outcome is the same as in eq.(11) and (12). Inverting the helicity of all the gluons, and taking the complex conjugates of the spinor products, we obtain the configurations with two positive-helicity gluons. In particular, we are interested in the configuration with gluons k_1 and k_2 having negative helicity. To that purpose, we first compute the amplitude for the configuration of Fig. 7d,

$$\begin{aligned} & M(-p_A, +; p'_A, -; k_1, +; k_2, +; p'_B, -; -p_B, +) \qquad (55) \\ & = \left(\frac{p'_{B\perp}}{p'^*_{B\perp}} \right)^2 M(-p_A, -; p'_A, +; k_1, +; k_2, +; p'_B, +; -p_B, -)\,, \end{aligned}$$

and then we reverse all the helicities (Fig. 7e), i.e. we take in eq.(55) the complex conjugates of the spinor products. Thus we obtain the amplitude for the configuration $(-p_A, -; p'_A, +; k_1, -; k_2, -; p'_B, +; -p_B, -)$ in the form of eq.(44), with $C_{-+}(-p_A, p'_A)$

and $C_{-+}(-p_B, p'_B)$ given in eq.(45), and $A_{--}(k_1, k_2) = A^*_{++}(k_1, k_2)$ and $B_{--}(k_1, k_2) = B^*_{++}(k_1, k_2)$ derived from eq.(49) and (51). By taking then the multi-Regge limit of eq.(44) with $\nu_1 = \nu_2 = +$ and $\nu_1 = \nu_2 = -$, we obtain

$$\begin{aligned} &\lim_{y_1 \gg y_2} M(-p_A, -; p'_A, +; k_1, -; k_2, -; p'_B, +; -p_B, -) \\ &= \frac{p'_{A\perp} k_{1\perp} k_{2\perp} p'^*_{B\perp}}{p'^*_{A\perp} k^*_{1\perp} k^*_{2\perp} p'_{B\perp}} \lim_{y_1 \gg y_2} M(-p_A, -; p'_A, +; k_1, +; k_2, +; p'_B, +; -p_B, -)\,, \end{aligned} \tag{56}$$

in agreement with eq.(13), iterated two times. Again, the other helicity configurations of eq.(47) are obtained by substituting the product $[p_A p_B]^4$ with the suitable product according to the pair of positive-helicity gluons considered, and the outcome is the same as in eq.(11) and (12).

In an analogous way to the generalization of the kinematics (16) to the production of $n + 2$ gluons, with 2 gluons in a forward-rapidity region, done at the end of sect. 3.1, we may generalize the amplitude (44) in the helicity configuration of Fig. 7a to the production of $n + 2$ gluons, with 2 gluons with likewise rapidity in the central-rapidity region. As in sect. 3.1, the color counting yields $3!2^n$ leading color orderings, which for $n = 2$ gives the 24 orderings considered in eq.(44).

4.2 The amplitudes with 3 negative-helicity gluons

The other helicity configurations we are interested in are the ones where gluons k_1 and k_2 have opposite helicities (Fig. 7f, g). In the multi-Regge kinematics, and in the next-to-leading corrections to it (43), helicity is conserved in the forward-rapidity regions (47) and two of the gluons emitted there must have negative helicity. Thus we need the subamplitudes in eq.(14) to have 3 negative and 3 positive-helicity gluons. These have been computed in ref. [15], [16], and are given in terms of 3 inequivalent helicity orderings: $(++-+--)$, $(+-+-+-)$ and $(+++---)$, singled out according to the color ordering. The subamplitudes may be written as [16],

$$\begin{aligned}
i\, m(p_1;p_2;p_3;p_4;p_5;p_6) \;&=\; 8\, i\, g^4 \left(\frac{\alpha^2}{\hat{t}_{123}\hat{s}_{12}\hat{s}_{23}\hat{s}_{45}\hat{s}_{56}} + \frac{\beta^2}{\hat{t}_{234}\hat{s}_{23}\hat{s}_{34}\hat{s}_{56}\hat{s}_{61}} \right. \\
&+ \left. \frac{\delta^2}{\hat{t}_{345}\hat{s}_{34}\hat{s}_{45}\hat{s}_{61}\hat{s}_{12}} + \frac{\hat{t}_{123}\,\beta\delta + \hat{t}_{234}\,\delta\alpha + \hat{t}_{345}\,\alpha\beta}{\hat{s}_{12}\hat{s}_{23}\hat{s}_{34}\hat{s}_{45}\hat{s}_{56}\hat{s}_{61}} \right) , \qquad (57) \\
\text{with} \qquad & \hat{t}_{ijk} = (p_i + p_j + p_k)^2 = \hat{s}_{ij} + \hat{s}_{jk} + \hat{s}_{ik}\, .
\end{aligned}$$

The coefficients α, β and δ for the different helicity orderings are,

	$1^+2^+3^+4^-5^-6^-$	$1^+2^+3^-4^+5^-6^-$	$1^+2^-3^+4^-5^+6^-$
α	0	$-[12]\langle 56\rangle\langle 4+\|\gamma\cdot K\|3+\rangle$	$[13]\langle 46\rangle\langle 5+\|\gamma\cdot K\|2+\rangle$
β	$[23]\langle 56\rangle\langle 1+\|\gamma\cdot K\|4+\rangle$	$[24]\langle 56\rangle\langle 1+\|\gamma\cdot K\|3+\rangle$	$[51]\langle 24\rangle\langle 3+\|\gamma\cdot K\|6+\rangle$
δ	$[12]\langle 45\rangle\langle 3+\|\gamma\cdot K\|6+\rangle$	$[12]\langle 35\rangle\langle 4+\|\gamma\cdot K\|6+\rangle$	$[35]\langle 62\rangle\langle 1+\|\gamma\cdot K\|4+\rangle$

(58)

$K = p_l + p_m + p_n$, with l, m, n the gluons with positive helicity.

We are interested in the configuration $(-p_A, -; p'_A, +; k_1, +; k_2, -; p'_B, +; -p_B, -)$. We begin to examine it in the color ordering $[A, A', 1, 2, B', B]$ (Fig. 8a), which is in the helicity ordering $(p'_A, +; k_1, +; k_2, -; p'_B, +; -p_B, -; -p_A, -)$. Then the subamplitude (57) has the form,

$$\begin{aligned}
&\text{coeff. of tr}\left(\lambda^a\lambda^{a'}\lambda^{d_1}\lambda^{d_2}\lambda^{b'}\lambda^b\right) \equiv -4\, i\, g^4\, \frac{\hat{s}}{|p'_{A\perp}|^2 |p'_{B\perp}|^2}\, C_{-+}(-p_B, p'_B)\, A_{+-}(k_1, k_2) \\
&= 8\, i\, g^4 \left(\frac{\alpha^2}{\hat{t}_{A'12}\hat{s}_{A'1}\hat{s}_{12}\hat{s}_{B'B}\hat{s}_{BA}} + \frac{\beta^2}{\hat{t}_{12B'}\hat{s}_{12}\hat{s}_{2B'}\hat{s}_{BA}\hat{s}_{AA'}} \right. \qquad (59) \\
&+ \left. \frac{\delta^2}{\hat{t}_{2B'B}\hat{s}_{2B'}\hat{s}_{B'B}\hat{s}_{AA'}\hat{s}_{A'1}} + \frac{\hat{t}_{A'12}\,\beta\delta + \hat{t}_{12B'}\,\delta\alpha + \hat{t}_{2B'B}\,\alpha\beta}{\hat{s}_{A'1}\hat{s}_{12}\hat{s}_{2B'}\hat{s}_{B'B}\hat{s}_{BA}\hat{s}_{AA'}} \right) ,
\end{aligned}$$

with the C-vertex given in eq.(45), the Mandelstam invariants taken from eq.(116) (Appendix D), and

$$\alpha \;=\; -[p'_A k_1]\,\langle p_B p_A\rangle\,\langle p'_B + |\gamma\cdot(p'_A + k_1 + p'_B)|k_2+\rangle$$

$$\begin{aligned}\beta &= [k_1 p'_B]\,\langle p_B p_A\rangle\,\langle p'_A + |\gamma\cdot(p'_A + k_1 + p'_B)|k_2 +\rangle \\ \delta &= [p'_A k_1]\,\langle k_2 p_B\rangle\,\langle p'_B + |\gamma\cdot(p'_A + k_1 + p'_B)|p_A +\rangle\end{aligned} \tag{60}$$

from eq.(58). Using the spinor products (89) (Appendix A) and (117) (Appendix D), and the identity (91) (Appendix A), we compute the coefficients (60) and the invariants $\hat{t}_{ijk}$ in the kinematics of eq.(43). In particular, $\hat{t}_{2B'B}$ is

$$\hat{t} \equiv \hat{t}_{2B'B} = (k_2 + p'_B - p_B)^2 = \hat{t}_{1AA'} \simeq -\left(|p'_{B\perp} + k_{2\perp}|^2 + k_1^- k_2^+\right)\,. \tag{61}$$

Thus the vertex A_{-+} in eq.(59) becomes,

$$\begin{aligned}A_{+-}(k_1,k_2) &= -2\,\frac{k_{1\perp}^*}{k_{1\perp}}\left\{-\frac{1}{\hat{s}_{12}}\left[\frac{k_{2\perp}^2|q_{A\perp}|^2}{(k_1^- + k_2^-)k_2^+} + \frac{k_{1\perp}^2|q_{B\perp}|^2}{(k_1^+ + k_2^+)k_1^-} + \frac{\hat{t}\,k_{1\perp}k_{2\perp}}{k_1^- k_2^+}\right]\right. \\ &+ \left.\frac{(q_{B\perp} + k_{2\perp})^2}{\hat{t}} - \frac{q_{B\perp} + k_{2\perp}}{\hat{s}_{12}}\left[\frac{k_1^- + k_2^-}{k_1^-}k_{1\perp} - \frac{k_1^+ + k_2^+}{k_2^+}k_{2\perp}\right]\right\} \\ \text{with} &\qquad q_A = -(p'_A - p_A) \qquad q_B = p'_B - p_B\,.\end{aligned} \tag{62}$$

Note that besides the usual pole as gluons 1 and 2 become collinear, eq.(62) has a 3-particle pole as $\hat{t} \to 0$, i.e. the amplitude factorizes into two subamplitudes connected by the propagator of the gluon exchanged between gluons 1 and 2. To obtain the coefficient of the color ordering $[A, A', 2, 1, B', B]$ (Fig. 8b), we must take the helicity ordering $(-p_B, -; -p_A, -; p'_A, +; k_2, -; k_1, +; p'_B, +)$. This is obtained from $(-p_B, +; -p_A, +; p'_A, -; k_2, +; k_1, -; p'_B, -)$ by reversing the helicities, i.e. by taking the complex conjugates of the corresponding spinor products, through the identities (91) and (92) (Appendix A). As we see from the direct calculation, it amounts to exchange the labels 1 and 2 and take the complex conjugate in eq.(62),

$$\text{coeff. of tr}\left(\lambda^a\lambda^{a'}\lambda^{d_2}\lambda^{d_1}\lambda^{b'}\lambda^b\right) = -4\,i\,g^4\,\frac{\hat{s}}{|p'_{A\perp}|^2|p'_{B\perp}|^2}\,C_{-+}(-p_B, p'_B)\,A^*_{+-}(k_2, k_1)\,. \tag{63}$$

In order to compute the coefficient of the color ordering $[A, A', 1, 2, B, B']$, obtained by taking gluon B' to the back of lego plot (Fig. 9a), we must consider the helicity ordering $(k_2, -; -p_B, -; p'_B, +; -p_A, -; p'_A, +; k_1, +)$, which is obtained from $(k_2, +; -p_B, +; p'_B, -; -p_A, +; p'_A, -; k_1, -)$ by reversing the helicities. For the color ordering $[A, 1, 2, B', B, A']$ (Fig. 9c), we must take the helicity ordering $(p'_A, +; -p_A, -; k_1, +; k_2, -; p'_B, +; -p_B, -)$ and α, β and δ from the third column of eq.(58); while for the color ordering $[A, 1, 2, B, B', A']$ (Fig. 10a) we consider the helicity ordering $(p'_B, +; p'_A, +; -p_A, -; k_1, +; k_2, -; -p_B, -)$. To the required accuracy we obtain,

$$\begin{aligned} &\text{coeff. of tr}\left(\lambda^a\lambda^{a'}\lambda^{d_1}\lambda^{d_2}\lambda^b\lambda^{b'}\right) = \text{coeff. of tr}\left(\lambda^a\lambda^{d_1}\lambda^{d_2}\lambda^{b'}\lambda^b\lambda^{a'}\right) \qquad (64)\\ &= -\text{coeff. of tr}\left(\lambda^a\lambda^{d_1}\lambda^{d_2}\lambda^b\lambda^{b'}\lambda^{a'}\right) = -\text{coeff. of tr}\left(\lambda^a\lambda^{a'}\lambda^{d_1}\lambda^{d_2}\lambda^{b'}\lambda^b\right) . \end{aligned}$$

For the color ordering $[A, A', 1, B', B, 2]$, obtained by taking gluon 2 to the back of lego plot (Fig. 9e), we take the helicity ordering $(p'_A, +; k_1, +; p'_B, +; -p_B, -; k_2, -; -p_A, -)$, for which the subamplitude has the simpler form,

$$\begin{aligned} &\text{coeff. of tr}\left(\lambda^a\lambda^{a'}\lambda^{d_1}\lambda^{b'}\lambda^b\lambda^{d_2}\right) \equiv 4\,i\,g^4\,\frac{\hat{s}}{|p'_{A\perp}|^2|p'_{B\perp}|^2}\,C_{-+}(-p_B, p'_B)\,B_{+-}(k_1, k_2) \qquad (65)\\ &= 8\,i\,g^4\left(\frac{\beta^2}{\hat{t}_{1BB'}\,\hat{s}_{1B'}\hat{s}_{B'B}\hat{s}_{2A}\hat{s}_{AA'}} + \frac{\delta^2}{\hat{t}_{B'B2}\hat{s}_{B'B}\hat{s}_{B2}\hat{s}_{AA'}\hat{s}_{A'1}} + \frac{\hat{t}_{A'1B'}\,\beta\delta}{\hat{s}_{A'1}\hat{s}_{1B'}\hat{s}_{B'B}\hat{s}_{B2}\hat{s}_{2A}\hat{s}_{AA'}}\right) ,\\ &\text{with}\quad \hat{t}_{1B'B} = (k_1 + p'_B - p_B)^2 = \hat{t}_{2AA'} = \simeq -\left(|p'_{B\perp} + k_{1\perp}|^2 + k_1^+k_2^-\right) , \end{aligned}$$

and β and δ given by the first column of eq.(58). After substitution of the spinor products and of the Mandelstam invariants we obtain,

$$B_{+-}(k_1, k_2) = -2\left[\frac{k_{2\perp}(q^*_{B\perp} + k^*_{1\perp})^2}{k^*_{2\perp}\hat{t}_{1B'B}} + \frac{k^*_{1\perp}(q_{B\perp} + k_{2\perp})^2}{k_{1\perp}\hat{t}_{2B'B}} + \frac{(q^*_{B\perp} + k^*_{1\perp})(q_{B\perp} + k_{2\perp})}{k_{1\perp}k^*_{2\perp}}\right] . \qquad (66)$$

Analogously to eq.(51), eq.(66) has no massless divergence when gluons 1 and 2 become collinear, since they are on opposite sides of the lego plot. In addition, it is invariant under the exchange of the labels 1 and 2 and the complex conjugation, and one can see that

$$B_{+-}(k_1,k_2) = A_{+-}(k_1,k_2) + A^*_{+-}(k_2,k_1)\,, \tag{67}$$

with $A_{+-}(k_1,k_2)$ given in eq.(62). Finally, for the color ordering $[A,A',1,B,B',2]$ (Fig. 10c) we take the helicity ordering $(p'_A,+;k_1,+;-p_B,-;p'_B,+;k_2,-;-p_A,-)$ and eq.(57) with α, β and δ given by the second column of eq.(58). However, the additional terms which appear with respect to eq.(65) are subleading to the required accuracy, and we obtain,

$$\text{coeff. of tr}\left(\lambda^a\lambda^{a'}\lambda^{d_1}\lambda^b\lambda^{b'}\lambda^{d_2}\right) = -\text{coeff. of tr}\left(\lambda^a\lambda^{a'}\lambda^{d_1}\lambda^{b'}\lambda^b\lambda^{d_2}\right)\,. \tag{68}$$

The coefficients of all the color orderings other than the ones of eq.(59), (64), (65) and (68) are subleading, and collecting the results of eq.(59) and (62-68) we obtain the amplitude for the configuration $(-p_A,-;p'_A,+;k_1,+;k_2,-;p'_B,+;-p_B,-)$ in the form of eq.(44), with $C_{-+}(-p_A,p'_A)$, $C_{-+}(-p_B,p'_B)$, $A_{+-}(k_1,k_2)$ and $B_{+-}(k_1,k_2)$ given in eq.(45), (62) and (66) respectively. In addition, for the color orderings obtained by exchanging gluons 1 and 2 the related coefficients undergo the complex conjugation, as shown in eq.(63) and summarized by eq.(46). By taking then the multi-Regge limit of eq.(44) with $\nu_1=\nu_2=+$ and $\nu_1=+$, $\nu_2=-$, we obtain

$$\begin{aligned}&\lim_{y_1\gg y_2} M(-p_A,-;p'_A,+;k_1,+;k_2,-;p'_B,+;-p_B,-) \\ &= \frac{(p'_{A\perp}+k_{1\perp})k_{2\perp}p'^*_{B\perp}}{(p'^*_{A\perp}+k^*_{1\perp})k^*_{2\perp}p'_{B\perp}} \lim_{y_1\gg y_2} M(-p_A,-;p'_A,+;k_1,+;k_2,+;p'_B,+;-p_B,-)\,,\end{aligned} \tag{69}$$

which, setting $p'_{A\perp}+k_{1\perp}=-q_{2\perp}$ and $p'_{B\perp}=q_{3\perp}$, is in agreement with eq.(13).

The other configuration of interest is $m(-p_A,-;p'_A,+;k_1,-;k_2,+;p'_B,+;-p_B,-)$. Using again eq.(57) and (58), we find that,

$$\begin{aligned}
\text{coeff. of tr}\left(\lambda^a\lambda^{a'}\lambda^{d_1}\lambda^{d_2}\lambda^{b'}\lambda^b\right) &= -4\,i\,g^4\,\frac{\hat{s}}{|p'_{A\perp}|^2|p'_{B\perp}|^2}\,C_{-+}(-p_B,p'_B)\,A^*_{+-}(k_1,k_2) \qquad (70)\\
\text{coeff. of tr}\left(\lambda^a\lambda^{a'}\lambda^{d_1}\lambda^{b'}\lambda^b\lambda^{d_2}\right) &= 4\,i\,g^4\,\frac{\hat{s}}{|p'_{A\perp}|^2|p'_{B\perp}|^2}\,C_{-+}(-p_B,p'_B)\,B^*_{+-}(k_1,k_2)\,,
\end{aligned}$$

with $A_{+-}(k_1,k_2)$ and $B_{+-}(k_1,k_2)$ defined in eq.(62) and (66), respectively. Accordingly the other leading color orderings may be computed, and we obtain the amplitude for the configuration $(-p_A,-;p'_A,+;k_1,-;k_2,+;p'_B,+;-p_B,-)$ in the form of eq.(44), with $A_{-+}(k_1,k_2)=A^*_{+-}(k_1,k_2)$ and $B_{-+}(k_1,k_2)=B^*_{+-}(k_1,k_2)$.

In this section we have explicitly considered the amplitudes in the configurations $(-p_A,-;p'_A,+;k_1,\pm;k_2,\mp;p'_B,+;-p_B,-)$. Accordingly, we may reverse the helicities of the gluons produced in the forward-rapidity regions, as in eq.(47). The effect of the reversal is the same as in eq.(11) and (12), i.e. it amounts to take the complex conjugate of the C-vertices in eq.(45). Thus each of the 16 leading helicity configurations of the 4-gluon production amplitude in the kinematics (43) may be cast in the form of eq.(44).

4.3 The Fadin-Lipatov amplitudes

The 4-gluon production amplitude, with gluons k_1 and k_2 produced in the central-rapidity region, according to the kinematics (43), has been computed in ref. [9], and for a generic helicity configuration is given by,

$$i\,M^{aa'd_1d_2b'b}_{\nu_A\nu'_A\nu_1\nu_2\nu'_B\nu_B} = 2\,i\,g^4\,\frac{\hat{s}}{\hat{s}_{AA'}\hat{s}_{BB'}}f^{a'ca}f^{b'c'b}\,\epsilon^{\nu_A *}_{\mu_A}(p_A)\epsilon^{\nu_B *}_{\mu_B}(p_B)\epsilon^{\nu'_A}_{\mu'_A}(p'_A)\epsilon^{\nu'_B}_{\mu'_B}(p'_B) \qquad (71)$$

$$\times\Gamma^{\mu_A\mu'_A}(p_A,p'_A,p_B)\,\Gamma^{\mu_B\mu'_B}(p_B,p'_B,p_A)\,\left[\epsilon^{\nu_1}_{\mu_1}(k_1)\epsilon^{\nu_2}_{\mu_2}(k_2)f^{cd_1j}f^{jd_2c'}A_{\mu_1\mu_2}+\left(\begin{array}{c} k_1\leftrightarrow k_2\\ \nu_1\leftrightarrow\nu_2\\ d_1\leftrightarrow d_2\end{array}\right)\right]\,,$$

where the Γ-tensors are given in eq.(3), the Mandelstam invariants in eq.(116) (Appendix D), and the 2-gluon production vertex A in the central-rapidity region is[3]

$$\begin{aligned}
A^{\mu_1\mu_2}(k_1,k_2) &= -\frac{a_1^{\mu_1}a_2^{\mu_2}}{\hat{t}}+\frac{b_1^{\mu_1}b_2^{\mu_2}}{\hat{s}}\left(1+\frac{k_1^-k_2^+}{\hat{t}}\right)-\frac{b_1^{\mu_1}c_2^{\mu_2}}{\hat{s}}\left(\frac{p'^+_Bp_A^+}{k_2^+(k_1^++k_2^+)}+\frac{p_A^+k_1^-k_2^-}{p_B^-\hat{t}}\right)\\
&-\frac{c_1^{\mu_1}b_2^{\mu_2}}{\hat{s}}\left(\frac{p'^-_Ap_B^-}{k_1^-(k_1^-+k_2^-)}+\frac{p_B^-k_1^+k_2^+}{p_A^+\hat{t}}\right)-\frac{c_1^{\mu_1}c_2^{\mu_2}}{\hat{s}}\left(1+\frac{\hat{s}_{12}}{\hat{t}}-\frac{k_1^+k_2^-}{\hat{t}}\right)\\
&-2\left(g^{\mu_1\mu_2}-\frac{2k_2^{\mu_1}k_1^{\mu_2}}{\hat{s}_{12}}\right)\\
&\times\left(1+\frac{\hat{t}}{\hat{s}_{12}}+\frac{k_1^-k_2^+}{\hat{t}}+\frac{k_1^-k_2^+-k_1^+k_2^-}{\hat{s}_{12}}+\frac{k_2^-}{k_1^-+k_2^-}\frac{p_A^+p'^-_A}{\hat{s}_{12}}+\frac{k_1^+}{k_1^++k_2^+}\frac{p_B^-p'^+_B}{\hat{s}_{12}}\right)\,,
\end{aligned}\tag{72}$$

with

$$\begin{aligned}
a_1 &= -2\left[-q_A+\left(\frac{k_1^+}{p_A^+}-\frac{p'^-_A}{k_1^-}\right)p_A-\frac{k_1^-}{p_B^-}p_B-\frac{\hat{t}}{\hat{s}_{12}}k_2\right]\\
a_2 &= -2\left[q_B+\left(\frac{k_2^-}{p_B^-}-\frac{p'^+_B}{k_2^+}\right)p_B-\frac{k_2^+}{p_A^+}p_A-\frac{\hat{t}}{\hat{s}_{12}}k_1\right]\\
b_1 &= 2\left(p_B-\frac{k_1^+p_B^-}{\hat{s}_{12}}k_2\right)\qquad b_2=2\left(p_A-\frac{p_A^+k_2^-}{\hat{s}_{12}}k_1\right)\\
c_1 &= 2\left(p_A-\frac{p_A^+k_1^-}{\hat{s}_{12}}k_2\right)\qquad c_2=2\left(p_B-\frac{k_2^+p_B^-}{\hat{s}_{12}}k_1\right)
\end{aligned}\tag{73}$$

and $\hat{t}$ and $q_{A,B}$ defined in eq.(61) and (62). Rewriting the product of structure constants as a trace of nested commutators (9), eq.(71) becomes

$$i\,M^{aa'd_1d_2b'b}_{\nu_A\nu'_A\nu_1\nu_2\nu'_B\nu_B}=-4\,i\,g^4\,\frac{\hat{s}}{\hat{s}_{AA'}\hat{s}_{BB'}}\epsilon^{\nu_A*}_{\mu_A}(p_A)\epsilon^{\nu_B*}_{\mu_B}(p_B)\epsilon^{\nu'_A}_{\mu'_A}(p'_A)\epsilon^{\nu'_B}_{\mu'_B}(p'_B)\epsilon^{\nu_1}_{\mu_1}(k_1)\epsilon^{\nu_2}_{\mu_2}(k_2)$$

---

[3] Eq.(72) is easily derived from the expression of A in ref. [9] by using the Mandelstam invariants (116) (Appendix D), or from the one in ref. [18] by writing the Sudakov variables in terms of the light-cone ones, $\beta_i=k_i^+/p_A^+$ and $\alpha_i=k_i^-/p_B^-$.

$$\begin{aligned}
&\times\Gamma^{\mu_A\mu'_A}(p_A,p'_A,p_B)\,\Gamma^{\mu_B\mu'_B}(p_B,p'_B,p_A)\,\left\{A_{\mu_1\mu_2}(k_1,k_2)\right.\\
&\times\Big[\mathrm{tr}\left(\lambda^a\lambda^{a'}\lambda^{d_1}\lambda^{d_2}\lambda^{b'}\lambda^b-\lambda^a\lambda^{a'}\lambda^{d_1}\lambda^{d_2}\lambda^b\lambda^{b'}-\lambda^a\lambda^{d_1}\lambda^{d_2}\lambda^{b'}\lambda^b\lambda^{a'}+\lambda^a\lambda^{d_1}\lambda^{d_2}\lambda^b\lambda^{b'}\lambda^{a'}\right)\\
&+\text{traces in reverse order}\Big]-\left[A_{\mu_1\mu_2}(k_1,k_2)+A_{\mu_2\mu_1}(k_2,k_1)\right]\\
&\times\Big[\mathrm{tr}\left(\lambda^a\lambda^{a'}\lambda^{d_1}\lambda^{b'}\lambda^b\lambda^{d_2}-\lambda^a\lambda^{a'}\lambda^{d_1}\lambda^b\lambda^{b'}\lambda^{d_2}\right)+\text{traces in reverse order}\Big]+\left.(1\leftrightarrow 2)\right\}\,.
\end{aligned}\tag{74}$$

Eq.(71), or (74), describes 16 helicity configurations, two for each of the produced gluons, since the helicity is conserved by the Γ-tensors in the forward-rapidity regions. The gluon polarizations are chosen like in eq.(95) (Appendix A), and the contractions of the Γ-tensors with the gluon polarizations are given by eq.(8). Eq.(74) becomes,

$$\begin{aligned}
&i\,M^{aa'd_1d_2b'b}_{\nu_A\nu'_A\nu_1\nu_2\nu'_B\nu_B}\\
&=-4\,i\,g^4\,\frac{\hat{s}}{|p'_{A\perp}|^2|p'_{B\perp}|^2}\,C_{\nu_A\nu'_A}(p_A,p'_A)\,C_{\nu_B\nu'_B}(p_B,p'_B)\,\epsilon^{\nu_1}_{\mu_1}(k_1)\epsilon^{\nu_2}_{\mu_2}(k_2)\left\{A_{\mu_1\mu_2}(k_1,k_2)\right.\\
&\times\Big[\mathrm{tr}\left(\lambda^a\lambda^{a'}\lambda^{d_1}\lambda^{d_2}\lambda^{b'}\lambda^b-\lambda^a\lambda^{a'}\lambda^{d_1}\lambda^{d_2}\lambda^b\lambda^{b'}-\lambda^a\lambda^{d_1}\lambda^{d_2}\lambda^{b'}\lambda^b\lambda^{a'}+\lambda^a\lambda^{d_1}\lambda^{d_2}\lambda^b\lambda^{b'}\lambda^{a'}\right)\\
&+\text{traces in reverse order}\Big]-\left[A_{\mu_1\mu_2}(k_1,k_2)+A_{\mu_2\mu_1}(k_2,k_1)\right]\\
&\times\Big[\mathrm{tr}\left(\lambda^a\lambda^{a'}\lambda^{d_1}\lambda^{b'}\lambda^b\lambda^{d_2}-\lambda^a\lambda^{a'}\lambda^{d_1}\lambda^b\lambda^{b'}\lambda^{d_2}\right)+\text{traces in reverse order}\Big]+\left.(1\leftrightarrow 2)\right\}\,,
\end{aligned}\tag{75}$$

with the C-vertices defined like in eq.(45),

$$\begin{aligned}
C_{++}(p_A,p'_A)&=&C_{--}(p_A,p'_A)=1\\
C_{++}(p_B,p'_B)&=&\frac{p'^*_{B\perp}}{p'_{B\perp}}\qquad C_{--}(p_B,p'_B)=C^*_{++}(p_B,p'_B)\,.
\end{aligned}\tag{76}$$

The choice of reference vectors is arbitrary since the amplitude (71) is gauge invariant, so for the gluons k_1 and k_2 we choose the polarizations $\epsilon^\nu_\mu(k_1,p_A)$ and $\epsilon^\nu_\mu(k_2,p_B)$. In the A-vertex (72) it is convenient to contract first the vectors a_1,b_1,c_1 (73) with the gluon polarization $\epsilon^\mu_L(k_1)$ (96) (Appendix A), and the vectors a_2,b_2,c_2 with $\epsilon^\mu_R(k_2)$, which yields the A-vertex in terms of transverse polarizations [18], and then to use the conversion (101) between the polarizations (95) and (96). We begin with the A-vertex having helicities $\nu_1 = \nu_2 = +$. Using eq.(99) (Appendix A), and after an appropriate amount of algebra we obtain,

$$A_{\mu_1\mu_2}(k_1,k_2)\epsilon^+_{\mu_1}(k_1,p_A)\epsilon^+_{\mu_2}(k_2,p_B) = A_{++}(k_1,k_2)\,, \tag{77}$$

with $A_{++}(k_1,k_2)$ defined in eq.(49). Setting $p'_{A\perp} = -q_{A\perp} \equiv -q_{1\perp}$ and $p'_{B\perp} = q_{B\perp} \equiv q_{2\perp}$, and using the contraction of the Lipatov vertex with the gluon polarizations (7), eq.(77) fulfills the multi-Regge limit,

$$\begin{aligned} \lim_{y_1 \gg y_2} A_{\mu_1\mu_2}\epsilon^+_{\mu_1}(k_1,p_A)\epsilon^+_{\mu_2}(k_2,p_B) &= -2\,\frac{q^*_{1\perp}q_{2\perp}}{k_{1\perp}k_{2\perp}} \\ &= C(q_1,q_{12})\cdot\epsilon^+(k_1)\,\frac{1}{\hat{t}_{12}}C(q_{12},q_2)\cdot\epsilon^+(k_2)\,, \end{aligned} \tag{78}$$

where q_{12} is the momentum of the gluon exchanged between k_1 and k_2 along the multi-Regge ladder, and $\hat{t}_{12} = -|q_{12\perp}|^2$. Exchanging then gluons k_1 and k_2 in eq.(77), we obtain $A_{\mu_1\mu_2}(k_2,k_1)\epsilon^+_{\mu_1}(k_2)\epsilon^+_{\mu_2}(k_1)$, which added to eq.(77) gives,

$$[A_{\mu_1\mu_2}(k_1,k_2) + A_{\mu_2\mu_1}(k_2,k_1)]\epsilon^+_{\mu_1}(k_1)\epsilon^+_{\mu_2}(k_2) = B_{++}(k_1,k_2)\,, \tag{79}$$

with $B_{++}(k_1,k_2)$ defined in eq.(51). Replacing eq.(77) and (79) into eq.(75) we obtain the amplitude for the configuration $(p_A,\nu_A;p'_A,\nu'_A;k_1,+;k_2,+;p'_B,\nu'_B;p_B,\nu_B)$, in agreement with its derivation eq.(44), with $\nu_1 = \nu_2 = +$, from the PT amplitudes (sect. 4.1). Taking then the complex conjugates of eq.(77) and (79) and substituting them into eq.(75), we obtain the amplitude in the configuration $(p_A,\nu_A;p'_A,\nu'_A;k_1,-;k_2,-;p'_B,\nu'_B;p_B,\nu_B)$, in agreement with eq.(44) with $\nu_1 = \nu_2 = -$.

The result of the contraction of the A-vertex with gluons k_1 and k_2 with opposite helicities is less simple. We obtain, after a bit of algebra,

$$A_{\mu_1\mu_2}(k_1,k_2)\epsilon^{+}_{\mu_1}(k_1,p_A)\epsilon^{-}_{\mu_2}(k_2,p_B) = A_{+-}(k_1,k_2)\,, \tag{80}$$

with $A_{+-}(k_1,k_2)$ defined in eq.(62). As a further check of eq.(77) and (80), we note that the amplitude (71) must not diverge more rapidly than $1/|q_{i\perp}|$ in the collinear regions $|q_{i\perp}| \to 0$, with $i = A, B$, in order for the related cross section not to diverge more than logarithmically [9]. However for $|q_{i\perp}| \to 0$, the amplitude (71) has poles due to the propagators $\hat{s}_{AA'} \simeq -|q_{A\perp}|^2$ and $\hat{s}_{BB'} \simeq -|q_{B\perp}|^2$, which entails that the A-vertex must be at least linear in $|q_{i\perp}|$,

$$\lim_{|q_{i\perp}|\to 0} A_{\mu_1\mu_2}(k_1,k_2)\epsilon^{\nu_1}_{\mu_1}(k_1,p_A)\epsilon^{\nu_2}_{\mu_2}(k_2,p_B) = O(|q_{i\perp}|) \tag{81}$$

with $i = A, B$, which is fulfilled by eq.(77) and (80).

Exchanging the labels 1 and 2 and taking the complex conjugate in eq.(80), we obtain $A_{\mu_1\mu_2}(k_2,k_1)\epsilon^{-}_{\mu_1}(k_2)\epsilon^{+}_{\mu_2}(k_1)$, which added to eq.(80) gives, after a bit of algebra,

$$[A_{\mu_1\mu_2}(k_1,k_2) + A_{\mu_2\mu_1}(k_2,k_1)]\epsilon^{+}_{\mu_1}(k_1)\epsilon^{-}_{\mu_2}(k_2) = B_{+-}(k_1,k_2)\,, \tag{82}$$

with $B_{+-}(k_1,k_2)$ defined in eq.(66). After substituting eq.(80) and (82) into eq.(75) we obtain the amplitude in the configuration $(p_A,\nu_A;p'_A,\nu'_A;k_1,+;k_2,-;p'_B,\nu'_B;p_B,\nu_B)$, in agreement with its derivation, eq.(44) with $\nu_1 = +$ and $\nu_2 = -$, from the helicity amplitudes with 3 negative-helicity gluons (sect. 4.2). Taking then the complex conjugates of eq.(80) and (82), we obtain the amplitude in the configuration $(p_A,\nu_A;p'_A,\nu'_A;k_1,-;k_2,+;p'_B,\nu'_B;p_B,\nu_B)$, in agreement with eq.(70).

5 Conclusions

Using the helicity formalism, we have computed the real next-to-leading corrections to the FKL amplitudes in the forward-rapidity region, eq.(17), and in the central-rapidity region, eq.(44); and we have shown that they are equivalent to the Fadin-Lipatov amplitudes, eq.(30) and (71) respectively, for the corresponding helicity configurations.

We note that the algebra involved in deriving eq.(17) and (44) is simpler starting from the helicity formalism than from the general expression of the Fadin-Lipatov amplitudes, eq.(30) and (71). This hints that even the real corrections beyond the next-to-leading order, which at the present time are known only formally [18], could be explicitly computed[4].

In addition, the computation of the square of the vertices for the production of two gluons with likewise rapidity in the forward-rapidity or in the central-rapidity regions [11], which is needed to evaluate the real next-to-leading logarithmic corrections to the kernel of the BFKL equation, is of course simpler starting from the amplitudes at fixed helicities, eq.(17) and (44), than from their general expression, eq.(30) and (71).

As remarked in the Introduction, in the next-to-leading corrections to the multi-Regge kinematics, and accordingly in the real next-to-leading logarithmic corrections to the kernel of the BFKL equation, also the production of a quark-antiquark pair with likewise rapidity in the forward-rapidity or in the central-rapidity regions contributes [10], [11]. The analysis of the corresponding amplitudes in the helicity formalism is left for the future.

---

[4] A formalism to compute the amplitude for the production of $n+2$ gluons with a cluster of m gluons, with $m \leq n+1$, in the forward-rapidity or in the central-rapidity regions, has been considered in ref. [18]. We merely note here that the corresponding color structures may be easily inferred from eq.(29) or from the generalization of eq.(44), and the color counting yields $(m+1)!\, 2^{n+2-m}$ leading color configurations.

Acknowledgements

I wish to thank Victor Fadin and Lev Lipatov for useful discussions.

A Multiparton kinematics

We consider the production of $n+2$ gluons of momentum p_i, with $i = 0, ..., n+1$ and $n \geq 0$, in the scattering between two gluons of momenta p_A and p_B. Using light-cone coordinates $p^\pm = p_0 \pm p_z$, and complex transverse coordinates $p_\perp = p_x + ip_y$, with scalar product $2p \cdot q = p^+ q^- + p^- q^+ - p_\perp q_\perp^* - p_\perp^* q_\perp$, the gluon 4-momenta are,

$$\begin{aligned} p_A &= \left(p_A^+, 0; 0, 0\right) , \\ p_B &= \left(0, p_B^-; 0, 0\right) , \\ p_i &= \left(|p_{i\perp}| e^{y_i}, |p_{i\perp}| e^{-y_i}; |p_{i\perp}| \cos\phi_i, |p_{i\perp}| \sin\phi_i\right) , \end{aligned} \tag{83}$$

where to the left of the semicolon we have the + and - components, and to the right the transverse components. y is the gluon rapidity and ϕ is the azimuthal angle between the vector $p_\perp$ and an arbitrary vector in the transverse plane. From the momentum conservation,

$$0 = \sum_{i=0}^{n+1} p_{i\perp} ,$$

$$\begin{aligned} p_A^+ &= \sum_{i=0}^{n+1} p_i^+\,, \qquad (84)\\ p_B^- &= \sum_{i=0}^{n+1} p_i^-\,, \end{aligned}$$

the Mandelstam invariants may be written as,

$$\begin{aligned} \hat{s} &= 2p_A\cdot p_B = \sum_{i,j=0}^{n+1} p_i^+ p_j^- \\ \hat{s}_{Ai} &= -2p_A\cdot p_i = -\sum_{j=0}^{n+1} p_i^- p_j^+ \qquad (85)\\ \hat{s}_{Bi} &= -2p_B\cdot p_i = -\sum_{j=0}^{n+1} p_i^+ p_j^- \\ \hat{s}_{ij} &= 2p_i\cdot p_j = p_i^+p_j^- + p_i^-p_j^+ - p_{i\perp}p_{j\perp}^* - p_{i\perp}^*p_{j\perp}\,. \end{aligned}$$

Massless Dirac spinors $\psi_\pm(p)$ of fixed helicity are defined by the projection,

$$\psi_\pm(p) = \frac{1\pm\gamma_5}{2}\psi(p)\,, \qquad (86)$$

with the shorthand notation,

$$\begin{aligned} \psi_\pm(p) &= |p\pm\rangle, \qquad \overline{\psi_\pm(p)} = \langle p\pm|\,, \\ \langle pk\rangle &= \langle p-|k+\rangle = \overline{\psi_-(p)}\psi_+(k)\,, \qquad (87)\\ [pk] &= \langle p+|k-\rangle = \overline{\psi_+(p)}\psi_-(k)\,. \end{aligned}$$

Using the spinor representation of ref. [5], we can write

$$\begin{aligned} \langle p_ip_j\rangle &= p_{i\perp}\sqrt{\frac{p_j^+}{p_i^+}} - p_{j\perp}\sqrt{\frac{p_i^+}{p_j^+}}\,, \\ \langle p_Ap_i\rangle &= -\sqrt{\frac{p_A^+}{p_i^+}}\,p_{i\perp}\,, \qquad (88) \end{aligned}$$

$$\begin{aligned}\langle p_i p_B\rangle &= -\sqrt{p_B^- p_i^+}\,,\\ \langle p_A p_B\rangle &= -\sqrt{\hat{s}}\,,\end{aligned}$$

where we have used the mass-shell condition $|p_{i\perp}|^2 = p_i^+ p_i^-$. We consider also the spinor products $\langle p_i + |\gamma\cdot p_k|p_j+\rangle$, which in the spinor representation of ref. [5] take the form,

$$\begin{aligned}\langle p_i + |\gamma\cdot p_k|p_j+\rangle &= \frac{1}{\sqrt{p_i^+ p_j^+}}\left(p_i^+ p_j^+ p_k^- - p_i^+ p_{j\perp} p_{k\perp}^* - p_{i\perp}^* p_j^+ p_{k\perp} + p_{i\perp}^* p_{j\perp} p_k^+\right)\\ \langle p_i + |\gamma\cdot p_j|p_A+\rangle &= \sqrt{\frac{p_A^+}{p_i^+}}\left(p_i^+ p_j^- - p_{i\perp}^* p_{j\perp}\right) \qquad (89)\\ \langle p_i + |\gamma\cdot p_j|p_B+\rangle &= \sqrt{\frac{p_B^-}{p_i^+}}\left(-p_i^+ p_{j\perp}^* + p_{i\perp}^* p_j^+\right)\,.\end{aligned}$$

The spinor products fulfill the identities,

$$\begin{aligned}\langle pk\rangle &= -\langle kp\rangle \qquad (90)\\ \langle pk\rangle^* &= [kp] \qquad (91)\\ (\langle p_i + |\gamma^\mu|p_j+\rangle)^* &= \langle p_j + |\gamma^\mu|p_i+\rangle \qquad (92)\\ \langle pk\rangle\,[kp] &= 2p\cdot k = |\hat{s}_{pk}|\,.\end{aligned}$$

Throughout the paper the following representation for the gluon polarization is used [17],

$$\epsilon_\mu^\pm(p,k) = \pm\frac{\langle p\pm|\gamma_\mu|k\pm\rangle}{\sqrt{2}\langle k\mp|p\pm\rangle}\,, \qquad (93)$$

which enjoys the properties

$$\begin{aligned}\epsilon_\mu^{\pm *}(p,k) &= \epsilon_\mu^\mp(p,k)\,,\\ \epsilon_\mu^\pm(p,k)\cdot p &= \epsilon_\mu^\pm(p,k)\cdot k = 0\,, \qquad (94)\\ \sum_{\nu=\pm}\epsilon_\mu^\nu(p,k)\epsilon_\rho^{\nu *}(p,k) &= -g_{\mu\rho} + \frac{p_\mu k_\rho + p_\rho k_\mu}{p\cdot k}\,,\end{aligned}$$

where k is an arbitrary light-like momentum. The sum in eq.(94) is equivalent to use an axial, or physical, gauge. We use the explicit representation of the gluon polarizations obtained in ref. [5],

$$\begin{aligned}
\epsilon_\mu^+(p_i,p_A) &= -\frac{p_{i\perp}^*}{p_{i\perp}}\left(\frac{\sqrt{2}\,p_{i\perp}}{p_i^-},0;\frac{1}{\sqrt{2}},\frac{i}{\sqrt{2}}\right)\,,\\
\epsilon_\mu^+(p_B,p_A) &= -\left(0,0;\frac{1}{\sqrt{2}},\frac{i}{\sqrt{2}}\right)\,,\\
\epsilon_\mu^+(p_A,p_B) &= \left(0,0;\frac{1}{\sqrt{2}},-\frac{i}{\sqrt{2}}\right)\,,\\
\epsilon_\mu^+(p_i,p_B) &= \left(0,\frac{\sqrt{2}\,p_{i\perp}^*}{p_i^+};\frac{1}{\sqrt{2}},-\frac{i}{\sqrt{2}}\right)\,,
\end{aligned} \tag{95}$$

in light-cone coordinates, and introduce the *left* and *right* physical gauges [4], defined respectively by the conditions $\epsilon_L(p)\cdot p_A=0$ and $\epsilon_R(p)\cdot p_B=0$. Accordingly, the decomposition of a polarization vector in light-cone or Sudakov components is,

$$\begin{aligned}
\epsilon_L^\mu(p) &= \epsilon_{L\perp}^\mu - \frac{p\cdot\epsilon_{L\perp}}{p\cdot p_A}\,p_A^\mu\,,\\
\epsilon_R^\mu(p) &= \epsilon_{R\perp}^\mu - \frac{p\cdot\epsilon_{R\perp}}{p\cdot p_B}\,p_B^\mu\,.
\end{aligned} \tag{96}$$

The polarizations $\epsilon_L^\mu(p)$, $\epsilon_R^\mu(p)$ for a momentum p not in the beam direction are related by a gauge tranformation,

$$\epsilon_R^\mu(p)=\epsilon_L^\mu(p)+2\,\frac{\epsilon_{L,\perp}\cdot p}{|p_\perp|^2}\,p^\mu\,, \tag{97}$$

which for the transverse components $\epsilon_{L\perp}^\mu$, $\epsilon_{R\perp}^\mu$ may be written as,

$$\epsilon_{R\perp}(p)=-\frac{p_\perp}{p_\perp^*}\epsilon_{L\perp}^*(p)\,. \tag{98}$$

We impose then the following standard polarizations,

$$\epsilon_{L\perp}^{\mu\pm}(p) = \left(0,0;\frac{1}{\sqrt{2}},\pm\frac{i}{\sqrt{2}}\right)\,, \tag{99}$$

$$\epsilon^{\mu\pm}_{L\perp}(p_B) = \epsilon^{\mu\mp}_{R\perp}(p_A) = \left(0, 0; \frac{1}{\sqrt{2}}, \pm\frac{i}{\sqrt{2}}\right) . \qquad (100)$$

We determine $\epsilon^{\mu}_{L}(p)$ using eq.(99) in the definition (96), then we find $\epsilon^{\mu}_{R}(p)$ using the gauge transformations (97) and (98) on $\epsilon^{\mu}_{L}(p)$. Finally, $\epsilon^{\mu}_{L}(p_B)$ and $\epsilon^{\mu}_{R}(p_A)$ are given by eq.(100) and the definitions (96). Comparing the results with eq.(95), we obtain the following conversion table among the representations (93) and (96) of the polarizations

$$\begin{aligned} \epsilon^{+}_{\mu}(p_i, p_A) &= -\frac{p^{*}_{i\perp}}{p_{i\perp}}\, \epsilon^{+}_{L\mu}(p_i) \,, \\ \epsilon^{+}_{\mu}(p_i, p_B) &= -\frac{p^{*}_{i\perp}}{p_{i\perp}}\, \epsilon^{+}_{R\mu}(p_i) \\ \epsilon^{+}_{\mu}(p_B, p_A) &= -\epsilon^{+}_{L\mu}(p_B) \,, \\ \epsilon^{+}_{\mu}(p_A, p_B) &= \epsilon^{+}_{R\mu}(p_A) \,. \end{aligned} \qquad (101)$$

B Multi-Regge kinematics

In the multi-Regge kinematics, we require that the gluons are strongly ordered in rapidity and have comparable transverse momentum (1),

$$y_0 \gg y_1 \gg ... \gg y_{n+1}; \qquad |p_{i\perp}| \simeq |p_\perp| \,. \qquad (102)$$

Momentum conservation (84) then becomes

$$\begin{aligned} 0 &= \sum_{i=0}^{n+1} p_{i\perp} \,, \\ p^{+}_{A} &\simeq p^{+}_{0} \,, \\ p^{-}_{B} &\simeq p^{-}_{n+1} \,. \end{aligned} \qquad (103)$$

The Mandelstam invariants (85) are reduced to,

$$\hat{s} = 2 p_A \cdot p_B \simeq p^{+}_{0} p^{-}_{n+1}$$

$$\begin{aligned}\hat{s}_{Ai} &= -2p_A\cdot p_i \simeq -p_0^+ p_i^- \\ \hat{s}_{Bi} &= -2p_B\cdot p_i \simeq -p_i^+ p_{n+1}^- \\ \hat{s}_{ij} &= 2p_i\cdot p_j \simeq |p_{i\perp}||p_{j\perp}|e^{|y_i-y_j|}\,,\end{aligned}\tag{104}$$

to leading accuracy. The spinor products (88) become,

$$\begin{aligned}\langle p_i p_j\rangle &\simeq -\sqrt{\frac{p_i^+}{p_j^+}}\,p_{j\perp} \qquad \text{for}\, y_i > y_j\,, \\ \langle p_A p_i\rangle &\simeq -\sqrt{\frac{p_0^+}{p_i^+}}\,p_{i\perp}\,, \\ \langle p_i p_B\rangle &\simeq -\sqrt{p_i^+ p_{n+1}^-}\,, \\ \langle p_A p_B\rangle &\simeq -\sqrt{p_0^+ p_{n+1}^-}\,.\end{aligned}\tag{105}$$

C Next-to-leading corrections in the forward-rapidity region

We consider the production of 3 gluons of momenta k_1, k_2 and p' in the scattering between two gluons of momenta k_0 and p, with gluon 4-momenta as given by eq.(83), with $k_0 \equiv p_A$ and $p \equiv p_B$. Gluons k_1 and k_2 are produced in the forward-rapidity region of gluon k_0 with likewise rapidity, and are separated by a large rapidity interval from p'. In addition, the produced gluons have comparable transverse momenta (16),

$$y_1 \simeq y_2 \gg y'\,; \qquad |k_{1\perp}| \simeq |k_{2\perp}| \simeq |p'_\perp|\,. \tag{106}$$

Momentum conservation (84) then yields,

$$0 = k_{1\perp} + k_{2\perp} + p'_\perp\,,$$

$$\begin{aligned} k_0^+ &\simeq k_1^+ + k_2^+ \,, \\ p^- &\simeq p'^- \,, \end{aligned} \tag{107}$$

and accordingly the Mandelstam invariants (85) may be written as,

$$\begin{aligned} \hat{s} &= 2k_0 \cdot p \,\simeq\, (k_1^+ + k_2^+)p'^- \,, \\ \hat{u} &= -2k_0 \cdot p' \,\simeq\, -(k_1^+ + k_2^+)p'^- \,, \\ \hat{u}_i &= -2p \cdot k_i \,\simeq\, -k_i^+ p'^- \,, \\ \hat{t}_i &= -2k_0 \cdot k_i \,\simeq\, -(k_1^+ + k_2^+)k_i^- \,, \\ \hat{t} &= -2p \cdot p' \,\simeq\, -|p'_\perp|^2 \,, \\ \hat{s}_{12} &= 2k_1 \cdot k_2 = k_1^+ k_2^- + k_1^- k_2^+ - k_{1\perp} k_{2\perp}^* - k_{1\perp}^* k_{2\perp} \,, \end{aligned} \tag{108}$$

to leading accuracy, with $i = 1, 2$. The spinor products (88) become

$$\begin{aligned} \langle k_0 p \rangle &= -\sqrt{\hat{s}} \simeq -\sqrt{(k_1^+ + k_2^+)p'^-} \,, \\ \langle k_0 p' \rangle &= -\sqrt{\frac{k_0^+}{p'^+}}\, p'_\perp \simeq \frac{p'_\perp}{|p'_\perp|} \langle k_0 p \rangle \,, \\ \langle k_0 k_i \rangle &= -\sqrt{\frac{k_0^+}{k_i^+}}\, k_{i\perp} \simeq -\sqrt{\frac{k_1^+ + k_2^+}{k_i^+}} k_{i\perp} \,, \\ \langle k_i p \rangle &= -\sqrt{p^- k_i^+} \,\simeq -\sqrt{k_i^+ p'^-} \,, \\ \langle p' p \rangle &= -\sqrt{p^- p'^+} \,\simeq -|p'_\perp| \,, \\ \langle k_i p' \rangle &= k_{i\perp} \sqrt{\frac{p'^+}{k_i^+}} - p'_\perp \sqrt{\frac{k_i^+}{p'^+}} \simeq -p'_\perp \sqrt{\frac{k_i^+}{p'^+}} \,, \\ \langle k_1 k_2 \rangle &= k_{1\perp} \sqrt{\frac{k_2^+}{k_1^+}} - k_{2\perp} \sqrt{\frac{k_1^+}{k_2^+}} \,, \end{aligned} \tag{109}$$

with $i = 1, 2$. From eq.(95), the gluon polarization vectors are

$$\begin{aligned}
\epsilon_\mu^+(p, k_0) &= -\left(0, 0; \frac{1}{\sqrt{2}}, \frac{i}{\sqrt{2}}\right) \\
\epsilon_\mu^+(k_0, p) &= \left(0, 0; \frac{1}{\sqrt{2}}, -\frac{i}{\sqrt{2}}\right) \\
\epsilon_\mu^+(p_i, k_0) &= -\frac{p_{i\perp}^*}{p_{i\perp}} \left(\frac{\sqrt{2}\, p_{i\perp}}{p_i^-}, 0; \frac{1}{\sqrt{2}}, \frac{i}{\sqrt{2}}\right) \\
\epsilon_\mu^+(p_i, p) &= \left(0, \frac{\sqrt{2}\, p_{i\perp}^*}{p_i^+}; \frac{1}{\sqrt{2}}, -\frac{i}{\sqrt{2}}\right) ,
\end{aligned} \tag{110}$$

with $p_i = k_1, k_2, p'$.

We straightforwardly extend the kinematics (16) to the production of $n + 2$ gluons of momenta k_1, k_2 and p_i, with $i = 1, ..., n$, in the scattering between two gluons of momenta k_0 and p, with gluons k_1 and k_2 in the forward-rapidity region of gluon k_0,

$$y_{k_1} \simeq y_{k_2} \gg y_{p_1} \gg ... \gg y_{p_n} ; \qquad |k_{1\perp}| \simeq |k_{2\perp}| \simeq |p_{i\perp}| , \tag{111}$$

with $1 = i, ..., n$. Momentum conservation (107) simply generalizes to,

$$\begin{aligned}
0 &= k_{1\perp} + k_{2\perp} + \sum_{i=1}^{n} p_{i\perp} , \\
k_0^+ &\simeq k_1^+ + k_2^+ , \\
p^- &\simeq p_n^- .
\end{aligned} \tag{112}$$

In the spinor products (109) we must replace the label p' with p_n, and consider the additional spinor products

$$\begin{aligned}
\langle k_0 p_i \rangle &= -\sqrt{\frac{k_0^+}{p_i^+}}\, p_{i\perp} \simeq -\sqrt{\frac{k_1^+ + k_2^+}{p_i^+}} p_{i\perp} , \\
\langle p_i p \rangle &= -\sqrt{p^- p_i^+} \simeq -\sqrt{p_i^+ p_n^-} ,
\end{aligned} \tag{113}$$

$$\langle k_j p_i\rangle = k_{j\perp}\sqrt{\frac{p_i^+}{k_j^+}} - p_{i\perp}\sqrt{\frac{k_j^+}{p_i^+}} \simeq -p_{i\perp}\sqrt{\frac{k_j^+}{p_i^+}}\,,$$

with $i = 1, ..., n-1$ and $j = 1, 2$.

D Next-to-leading corrections in the central-rapidity region

We consider the production of 4 gluons of momenta p'_A, k_1, k_2 and p'_B in the scattering between two gluons of momenta p_A and p_B. We require that gluons k_1 and k_2 have likewise rapidity and are produced far away from the forward-rapidity regions, with all the gluons having comparable transverse momenta,

$$y'_A \gg y_1 \simeq y_2 \gg y'_B\,; \qquad |k_{1\perp}| \simeq |k_{2\perp}| \simeq |p'_{A\perp}| \simeq |p'_{B\perp}|\,. \tag{114}$$

The momentum conservation has the same form as in the multi-Regge kinematics (103)

$$\begin{aligned} 0 &= p'_{A\perp} + k_{1\perp} + k_{2\perp} + p'_{B\perp} \\ p_A^+ &\simeq p'^+_A \\ p_B^- &\simeq p'^-_B\,. \end{aligned} \tag{115}$$

To leading accuracy, and except for $\hat{s}_{12}$, the Mandelstam invariants are the same as in the multi-Regge kinematics (104),

$$\begin{aligned} \hat{s} &= 2p_A\cdot p_B \simeq p'^+_A p'^-_B \\ \hat{s}_{AA'} &= -2p_A\cdot p'_A \simeq -|p'_{A\perp}|^2 \\ \hat{s}_{Ai} &= -2p_A\cdot k_i \simeq -p'^+_A k_i^- \end{aligned}$$

$$
\begin{aligned}
\hat{s}_{AB'} &= -2p_A \cdot p'_B \simeq -p'^{+}_A p'^{-}_B \\
\hat{s}_{BA'} &= -2p_B \cdot p'_A \simeq -p'^{+}_A p'^{-}_B \\
\hat{s}_{Bi} &= -2p_B \cdot k_i \simeq -k_i^+ p'^{-}_B \\
\hat{s}_{BB'} &= -2p_B \cdot p'_B \simeq -|p'_{B\perp}|^2 \\
\hat{s}_{A'i} &= 2p'_A \cdot k_i \simeq p'^{+}_A k_i^- \\
\hat{s}_{B'i} &= 2p'_B \cdot k_i \simeq k_i^+ p'^{-}_B \\
\hat{s}_{A'B'} &= 2p'_A \cdot p'_B \simeq p'^{+}_A p'^{-}_B \\
\hat{s}_{12} &= 2k_1 \cdot k_2 = k_1^+ k_2^- + k_1^- k_2^+ - k_{1\perp} k^*_{2\perp} - k^*_{1\perp} k_{2\perp} \,,
\end{aligned}
\tag{116}
$$

however, anytime a difference of invariants is taken such that the leading terms cancel, the invariants (116) must be determined to next-to-leading accuracy. The spinor products (88) become,

$$
\begin{aligned}
\langle p_A p_B \rangle &\simeq \langle p'_A p_B \rangle \simeq -\sqrt{p'^{+}_A p'^{-}_B} \\
\langle p_A p'_B \rangle &\simeq \langle p'_A p'_B \rangle = -\sqrt{\frac{p'^{+}_A}{p'^{+}_B}}\, p'_{B\perp} \\
\langle p_A k_i \rangle &\simeq \langle p'_A k_i \rangle = -\sqrt{\frac{p'^{+}_A}{k_i^+}}\, k_{i\perp} \\
\langle k_i p_B \rangle &\simeq -\sqrt{k_i^+ p'^{-}_B} \\
\langle k_i p'_B \rangle &\simeq -\sqrt{\frac{k_i^+}{p'^{+}_B}}\, p'_{B\perp} \\
\langle p_A p'_A \rangle &\simeq -p'_{A\perp} \\
\langle p'_B p_B \rangle &\simeq -|p'_{B\perp}| \\
\langle k_1 k_2 \rangle &= k_{1\perp}\sqrt{\frac{k_2^+}{k_1^+}} - k_{2\perp}\sqrt{\frac{k_1^+}{k_2^+}} \,.
\end{aligned}
\tag{117}
$$

References

[1] L.N. Lipatov, Yad. Fiz. **23**, 642 (1976) [Sov. J. Nucl. Phys. **23**, 338 (1976)].

[2] E.A. Kuraev, L.N. Lipatov and V.S. Fadin, Zh. Eksp. Teor. Fiz. **71**, 840 (1976) [Sov. Phys. JETP **44**, 443 (1976)].

[3] E.A. Kuraev, L.N. Lipatov and V.S. Fadin, Zh. Eksp. Teor. Fiz. **72**, 377 (1977) [Sov. Phys. JETP **45**, 199 (1977)];
Ya.Ya. Balitsky and L.N. Lipatov, Yad. Fiz. **28** 1597 (1978) [Sov. J. Nucl. Phys. **28**, 822 (1978)].

[4] L.N. Lipatov, Nucl. Phys. **B365**, 614 (1991).

[5] V. Del Duca, Phys. Rev. D **52**, 1527 (1995).

[6] S.J. Parke and T. Taylor, Phys. Rev. Lett. **56**, 2459 (1986).

[7] A. Bassetto, M. Ciafaloni and G. Marchesini, Phys. Rep. **100**, 201 (1983).

[8] A.H. Mueller and H. Navelet, Nucl. Phys. **B282**, 727 (1987).

[9] L.N. Lipatov and V.S. Fadin, Yad. Fiz. **50**, 1141 (1989) [Sov. J. Nucl. Phys. **50**, 712 (1989)].

[10] V.S. Fadin, R. Fiore and A. Quartarolo, Phys. Rev. D **50**, 2265, 5893 (1994).

[11] V.S. Fadin and L.N. Lipatov, in progress.

[12] V.S. Fadin and R. Fiore, Phys. Lett. **294B**, 286 (1992); V.S. Fadin and L.N. Lipatov, Nucl. Phys. **B406**, 259 (1993); V.S. Fadin, preprint BUDKERINP 94-103.

[13] G. Veneziano, Phys. Lett. **43B**, 413 (1973);
J.D. Bjorken, Phys. Rev. D **45**, 4077 (1992).

[14] V. Del Duca, Phys. Rev. D **48**, 5133 (1993).

[15] F.A. Berends and W. Giele, Nucl. Phys. **B294**, 700 (1987).

[16] M.L. Mangano, S.J. Parke and Z. Xu, Nucl. Phys. **B298**, 653 (1988).

[17] M.L. Mangano and S.J. Parke, Phys. Rep. **200**, 301 (1991).

[18] L.N. Lipatov, Nucl. Phys. **B452**, 369 (1995).